A Mechanistic Design Approach for Graphite Nanoplatelet Reinforced Asphalt Mixtures for Low Temperature Applications

A THESIS
SUBMITTED TO THE FACULTY OF THE GRADUATE SCHOOL
OF THE UNIVERSITY OF MINNESOTA
BY

Rebecca Hendrickson

IN PARTIAL FULFILLMENT OF THE REQUIREMENTS
FOR THE DEGREE OF
MASTER OF SCIENCE

Jia-Liang Le, advisor

May, 2017

Acknowledgements

I would like to thank Professor Jia-Liang Le for serving as my advisor for this project. I would also like to thank Professor Mihai Marasteanu for his assistance with obtaining materials and performing laboratory tests and I would like to thank Mugurel Turos for preforming the material tests in the University of Minnesota Pavement Lab. I would like to thank Itasca Consulting Group for the use of their computational model, PFC3D. I would also like to thank Derrick Blanksma with Itasca Consulting Group for his work as my mentor for the Itasca Educational Program and for his guidance with the computational program, PFC3D. Finally, I would like to thank MnDOT for providing me with funding for this research project and my master's degree.

Abstract

This thesis explores the application of a widely used commercial discrete computational model (PFC3D) for predicting the fracture behavior of asphalt mixtures at low temperatures using input parameters from simple experiments. In this discrete element model, coarse aggregates are explicitly represented by spheres, which are connected by bonds representing the fine aggregate mixture (i.e. asphalt binder with the fine-size aggregates). Bending beam rheometer tests are performed to obtain the mechanical properties of the fine aggregate mixture (FAM) at low temperatures. The model is then used to simulate the semi-circular bend (SCB) tests. The comparison between the simulated and experimental results on SCB tests shows that the PFC3D model could predict the peak load and post peak behavior of the SCB specimens if an appropriate scaling relation for the strength of FAM is taken into consideration. The post-peak behavior of the SCB specimens can only be captured by taking into account the energy required to fracture one bond which can not be directly obtained from experiments on the FAM and is a fitting pararmeter. A parametric study is performed to understand the influence of different model parameters of the PFC3D on the predicted behavior of SCB specimens.

Contents

List of Tables

List of Figures

Chapter 1

Introduction

Low temperature cracking in asphalt pavements is a widespread concern especially in the northern states. Such failures could significantly shorten the lifespan and affect the durability of the pavements, which usually lead to costly pavement repair and rehabilitation [1]. Over decades, there has been a sustained amount of effort devoted towards improving the performance of asphalt pavements. A major part of these efforts has been focused on the development of new asphalt-based pavement materials, in which asphalt binders are modified by polymers, nano-clay, nano-silica, carbon nanotubes, basalt fibers, and graphite nano-platelets [2, 3, 4, 5, 6]. Extensive laboratory experiments are required in order to understand the influence of these additives on the fracture behavior of asphalt mixtures. One potential means of reducing the experimental efforts is to rely on computational models to predict the fracture behavior of the mixtures based on the properties of asphalt binders, which could be measured in simple laboratory experiments.

In this study, we explore the application of a discrete element model for creating an essential representation of the behavior of asphalt mixtures at low temperatures. Compared to more sophisticated representations of the microstructure, in this model, only the coarse aggregates are modeled explicitly as random sized particles in order to improve the computational efficiency. The fine aggregates and asphalt binder are combined as fine aggregate mixtures (FAM), which are represented by the bonds between the coarse aggregates. This discrete element model requires only the essential material properties of the FAM versus models that explicitly model the binder, aggregates and

interface as particles, requiring material properties of the entire mixture. The mechanical properties of FAM are measured using bending beam rheometer (BBR) tests, based on which the discrete element model is used to predict the peak load for the fracture behavior of the asphalt mixtures. Since the input parameters can be obtained from BBR experiments on FAM, time consuming tests on the entire asphalt mixture are unnecessary for determining the peak load of the asphalt mixture. The post-peak behavior can be predicted using the bond fracture energy as a fitting parameters, which is a function of the parameters obtained from the BBR test. This research focuses on the low temperature behavior of the asphalt mixtures. Therefore, the viscoelastic response is ignored since the asphalt mixtures exhibit brittle behavior at low temperatures.

The thesis is planned as follows: Chapter 2 provides a summary of previous literature; Chapter 3 describes the model; Chapter 4 presents the preparation of the samples, the BBR test of the FAM and semi-circular bend (SCB) test of the mixtures; Chapter 5 presents the comparison between the simulation results and the experimental observations and a parametric study on how the parameters of the discrete element model would influence the mixture behavior, and Chapter 6 presents a final discussion on the analysis presented in this thesis.

Chapter 2

Literature Review

The application of nanotechnology for asphalt mixtures has shown many benefits. Various nanomaterials have been used to evaluate the performance of modified asphalt, specifically for resistance to cracking and other forms of failure. In a recent study at the University of Minnesota, researchers developed Graphite Nanoplatelet (GNP) reinforced asphalt binders and mixtures, which exhibit a significant improvement in mechanical properties at low temperatures. However, there is currently not a comprehensive approach for determining the optimum mix design of the reinforced asphalt binders and mixtures.

Although experimental test methods are indispensable for gaining insight into the behavior of nanomaterial-reinforced asphalt materials, these tests are usually very costly and time consuming, which makes them not ideal for identifying the optimum mix design. The use of computational modeling alongside lab results provides further understanding of the various physical mechanisms responsible for the observed behavior of the asphalt mixtures. The combination of computational and experimental investigations are advantageous for performing parametric studies to obtain the relationship between the mix design and the mechanical properties of asphalt mixtures with a minimum amount of laboratory testing.

The current efforts on the applications of nanotechnology in asphalt mixtures and noted the experimental tests that were utilized to obtain the findings were discussed. In addition, the two main computational methods that have been used for modeling the asphalt materials, namely the continuum approach and the discrete element method

have been summarized.

2.1 Nanomaterials

In recent years, there has been an emerging interest in applying nanotechnology to asphalt pavement materials. It was postulated that nanotechnology could potentially play a major role in the improved use of existing and available materials in pavements and in the material processing to improve the sustainability and resilience of the pavement [1]. A nanoparticle is defined as a particle with its least dimension being less than 100 nanometers [7]. Research has suggested that nanoclay, nanosilica, carbon nanotubes, basalt fibers and graphite nanoplatelets (GNPs) could lead to an improvement of the performance of the asphalt mixtures.

2.1.1 Nanoclays

Nanoclays are nanoparticles of layered mineral silicates. While being a naturally occurring inorganic material, nanoclay can be altered in order to make it compatible with organic monomers and polymers and has a layer thickness on the order of one nanometer [7, 8]. Compared to polymer-modified binder, nanoclays are relatively inexpensive since they are naturally occurring [9]. Not only are nanoclays a more cost efficient options, they also have favorable mechanical properties such as their nanoscopic size and surface area which have shown tendencies for increasing stiffness of asphalt binders [5].

Extensive research has been devoted towards the use of nanoclays to reinforce asphalt binders. Although some types of nanoclay did not affect the stiffness or viscosity of the bitumen, other types of nanoclay did show encouraging results [3]. Upon testing stiffness and tensile strength, tensile modulus, flexural strength and modulus thermal stability, it was found that, compared to unmodified bitumen, the elasticity increased for the nanoclay-modified bitumen while the dissipation of mechanical energy was lower [3, 10]. Bentonite clay (BT) and organically modified bentonite (OBT) were also used to reinforce asphalt binders in pavement mixtures. While analyzed under shearing stresses and sonication, the modified asphalts ultimately had a higher rutting resistance, which could improve the low temperature rheological properties of asphalt [3, 11].

In order to gain a better understanding into the benefits of nanoclay modified

binders, the nanostructure and microstructure as well as the mechanical behavior of asphalt clay nanocomposites has been investigated. Many atomic force microscopy (AFM) techniques were employed including tapping mode imaging, force spectroscopy and nanoindentation as well as X-ray diffraction (XRD) experiments. These techniques indicated that nanoclay had an exfoliated structure with enhanced adhesive forces [12]. Specific nanoscale properties like the state of dispersion and the exfoliation of the nanoclay binders have also been analyzed using techniques such as scanning electron microscopy (SEM) and (XRD) approaches [5]. Fourier transform infrared (FTIR) testing has also been employed to evaluate the interactions between nanoclay and asphalt [13]. The investigation of the nanoscale properties of the binders indicated that the improvement of the stiffness and hardness of the asphalt would depend on the temperature and percentage of nanoclay. These improvements appeared to result from the network of exfoliated nanoclay layers and the aggregates [12]. In general, the improvement of mechanical properties of the asphalt mixture can be better understood by the interactions of the aggregates and binders at a nanoscopic scale.

Recent studies with nanoclay-modified binders also showed an increase in the Superpave rutting factor and the rotational viscosity (RV) tests indicated a significant increase in viscosity. These results pointed toward nanoclay as an alternative to polymer-modified binders for more cost efficient pavement solutions and maintenance [5]. Meanwhile, dynamic mechanical analysis, flexural creep stiffness and flexural tests on nanoclay-modified binders indicted that the temperature susceptibility and complex modulus increase while the phase angle decrease [13]. Other laboratory methods including the surface free energy (SFE) and small angle X-ray diffraction (SACD) techniques have been applied to nanoclay-modified asphalt mixtures to investigate the moisture susceptibility properties of nanoclay-modified asphalt binders [9]. Among its other benefits, nanoclay has also been found to improve the aging resistance and storage-ability of asphalt mixtures [9, 14]

2.1.2 Nanosilica

Silica is also an abundant compound that has applications outside of material science in areas such as medication and drug distribution [3, 15]. Nanosilica has also been used to reinforce elastomers as a rheological solute. Similar to nanoclay, nanosilica

is beneficial due to its low cost of production and high performance [3]. Laboratory testing has found a slight decrease in viscosity values with the addition of nanosilica in asphalt. This indicates that the compaction temperatures would be lower or lower energy of the construction process will be achieved [3]. It was found that the addition of nanosilica could enhance anti-aging, fatigue cracking and rutting resistance and anti-stripping properties. Although beneficial in some aspects, the low temperature performance of nanosilica in asphalt binders was not remarkable. The stress relaxation capacity remained the same for nanosilica modified asphalt binders and in general, the low temperature properties of the asphalt binders were not greatly affected [3, 16].

Techniques used to analyze nanosilica-enhanced binders include morphological, rheological and thermal analysis techniques. Differential scanning calorimetry (DSC), thermogravimetric analysis (TGA), atomic force microscopy, and Fourier Transform Infrared spectroscopy (FTIR) were also used to quantify the effect of nanosilica as a binder modifier. The optimum content of the nanosilica modifier could be determined based primarily on the results from dynamic shear rheometer (DSR) asphalt fatigue and rutting tests [7]. Moisture susceptibility, resilient modulus, and dynamic creep tests were also employed to evaluate the performance of nanosilica particles added to polymer modified asphalt mixtures under different aging and moisture susceptibility conditions [17]. Scanning electron microscopy was used to analyze how well the particle dispersed into the asphalt binder. It was found that nanosilica could reduce the susceptibility to moisture damage and increase the strength as well as enhances the fatigue and rutting resistance of asphalt binders [17]. Additional laboratory tests include rotational viscosity (RV), bending beam rheometer (BBR), and flow number (FN) tests showing signs of an improved dynamic modulus, flow number and improved rutting and fatigue performance [17]. The results indicated that nanosilica produces beneficial results for asphalt pavement materials but does not specifically improve these materials under cold temperature conditions.

2.1.3 Carbon Nanotubes

Carbon nanotubes (CNT) are one-atom thin sheets of graphite shaped into a hollow cylinder [3]. Their diameter is on the order of one nanometer and CNTs have superior mechanical properties with high tensile strength [3]. Although there is less available

literature for the use of CNTs to reinforce asphalt binders, improvements have been documented. Most prominently investigated in two forms, single and double wall nanotubes have been analyzed using atomic force microscopy. When adding CNTs to asphalt, an increase in adhesive forces has been noted as well as an increase in moisture susceptibility [18]. The morphology of CNT-modified hot mix asphalt was also examined using scanning electron microscopy. The mechanical properties, including resilient modulus, creep behavior, and fatigue performance indicated that CNTs produced an improvement against fatigue and permanent deformation compared to conventional HMA [6]. Overall, CNTs have produced results to indicate enhanced rutting resistance potential and enhanced resistance to thermal cracking [3]. However, it was found that the dispersion of CNTs in asphalt binders represents a major challenge [19]. In order to achieve a good dispersion, the CNTs have to be added into some particular types of asphalt emulsions. With the relatively high material cost, the application of CNTs in asphalt pavements is rather limited. Basalt fiber is a material made from fine fibers of basalt, resembling carbon fiber and fiberglass. It is highly resistant to alkaline and salt creating potential use for concrete, bridge and shoreline structures [20]. Dynamic shear rheological tests and creep tests indicated that basalt fibers could lead to an improvement in the performance of asphalt binders [4]. Basalt fiber reinforced asphalt mixtures have demonstrated a high absorption ratio, low water absorption ratio and high tensile strength and temperature stability [4]. Fatigue properties of asphalt mixtures under complicated environment situations like low temperature bending performance, chloride penetration, freezing-thawing cycle and their coupling effects were studied for basalt fiber reinforced asphalt mixtures [21]. The optimum dosage of basalt fiber was determined using the Marshall test and the results indicate that the tensile strength, the maximum curving tensile stress, the curving stiffness modulus, and fatigue properties are influenced by the chloride erosion and freezing-thawing cycle [21]. Therefore low temperature-bending performance and fatigue properties of asphalt mixtures could be improved by adding moderate amounts of basalt fibers. The tensile strength of basalt fiber asphalt binder showed improvement using the results from the direct tension test [2]. Experimental results also indicated a reduction in failure stiffness and an overall improved of low temperature cracking resistance of asphalt concrete at low temperatures with basalt fiber reinforcement [22].

2.1.4 Graphite Nanoplateletes

Recent efforts have also been directed towards the application of the graphite nanoplatelets (GNPs) to asphalt binders and mixtures. The GNPs are produced from the exfoliated graphite (Figure 2.1), which has shown great mechanical and electron transport properties: the stiffness of graphite is on the order of 1 TPa, the strength of graphite is about 100 times that of steel, and the electric conductivity of graphite is somewhat higher than that of copper [23, 24, 25]. Furthermore, it has been shown that graphite has an exceptional thermal stability up to at least 2600K [26].

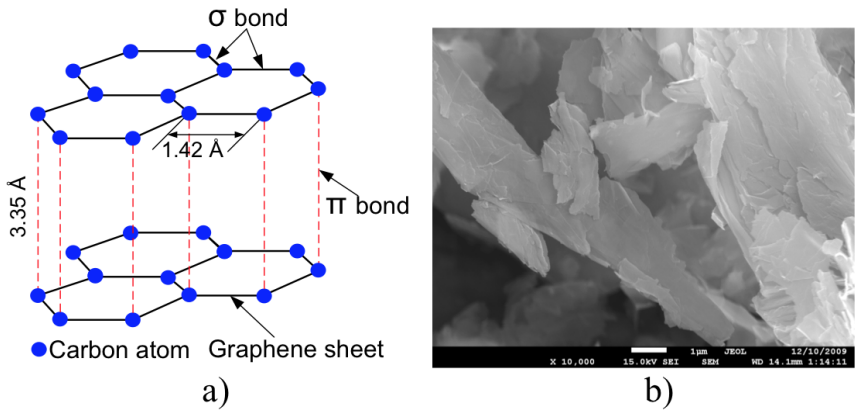

Figure 2.1: a) schematic of atomic structure of GNP, and b) SEM image of GNP.

Recent studies have shown that the GNP can be easily incorporated into asphalt binders, and due to its relatively low aspect ratio no potential clustering is observed during the mixing. The complex shear modulus test indicated that the addition of GNP into both the polymer-modified and unmodified asphalt binders almost does not affect the complex shear modulus and phase angle. Strength tests showed that the GNP-modified asphalt binders exhibit superior flexural strength at low temperatures compared to conventional asphalt binders. For both polymer-modified and unmodified asphalt binders, a moderate addition of GNP, i.e. 3% to 6% by weight of the binder, can lead to about 130% increase in flexural strength. Meanwhile, it was also observed that the addition of GNP could lead to an increase in the IDT strength and fracture energy of asphalt mixtures. Compared to the increase in flexural strength of GNP-modified

asphalt binders, this increase is less significant. The addition of GNP can effectively reduce the compaction effort of the asphalt mixtures, and meanwhile it can also improve the rutting performance of the mixtures.

2.2 Computational Models

Although experimental investigations provide a direct means of understanding of the mechanical properties of the nanomaterials and their interactions with asphalt mixtures, computational methods are particularly useful for the prediction of the behavior of asphalt binders and mixtures. Such predictive models are valuable in terms of reducing the costly experiments. To some extent, these models will allow us to perform experiments on computers, which are usually referred to as the simulation-based experiments. This concept has been developed for the design of various modern engineering structures, which experimental cost is prohibitively high. However, it has not been fully utilized for the design of asphalt mixtures.

The existing computational methods can be classified into two categories, which include the continuum approach and the discrete element method. The continuum approach provides efficient means of simulating the mechanical behavior of the asphalt mixtures, as it essentially smears the material inhomogeneity. By contrast, the discrete element method explicitly models the microstructure of the asphalt mixtures, which provides a more physical representation of the material, at the expense of a substantial higher requirement of the computational effort.

2.2.1 Finite Element Analysis

Many existing computational modeling of asphalt mixtures are essentially anchored by the use of the finite element (FE) approach. The FE method basically finds an approximate solution to boundary value problems for partial differential equations, allowing complex geometries to be accurately represented. The essence of FE simulations is to incorporate a realistic constitutive model for asphalt mixtures. In a recent study [27], a continuum-damage model was proposed to determine internal state variables that can be used to predict the locally averaged amount of damage in an asphalt sample. Figure 2.2 shows how this model can be used to represent the overall locally averaged

amount of damage to the asphalt sample where the individual aggregates are not modeled independently. Since the parameters are determined from testing specific samples, the continuum-damage mechanics model is specific to the type of mixture [28]. This approach takes into account the heterogeneous geometric characteristics and inelastic mechanical behavior of asphalt mixtures. With such a constitutive model, the FE model has been used to predict the damage and fracture of asphalt mixtures [28]. FEM can also incorporate the rate-dependent fracture failure properties alongside related experimental protocols. This model could help reduce experimental cost and time by achieving better insight into the properties of asphalt mixtures [29]. Beyond predicting failure in asphalt mixtures, the FE method has also been applied to model other physical processes, such as the progressive moisture damage behavior of asphalt [30]. Moisture damage due to water transport was incorporated with mechanical loading to simulate the nonlinear damage in the model. FEM could allow various parametric analyses to investigate how each of the parameters affects the moisture damage of that material [30]. The essence of FE simulations is to incorporate a realistic constitutive model for entire asphalt mixtures. A continuum-damage model was proposed to determine internal state variables that can be used to predict the locally averaged amount of damage in an asphalt sample [27]. Since the parameters are determined from testing specific samples, the continuum-damage mechanics model is specific to the type of mixture [28]. This approach takes into account the heterogeneous geometric characteristics and inelastic mechanical behavior of asphalt mixtures and with such a constitutive model, the FE model has been used to predict the damage and fracture of asphalt mixtures [28].

The FE model essentially takes a smeared damage approach, which does not explicitly model the discrete fracture behavior. In order to better model the material fracture, the cohesive zone fracture model (CZM) has been often used within the framework of FE analysis. The CZM was pioneered for ductile fracture in the 1960s [31, 32], and was later extended to quasibrittle fracture [24, 33]. The essential idea of CZM is that it uses a nonlinear element to represent the fracture process zone at the crack tip, where the other part of the structure is treated as linearly elastic. Figure 2.3 demonstrates how the discrete cracks can be modeled by cohesive zones [28]. Similarly, Figure 2.3 also indicates the use of the cohesive zone model for reproducing the damage of the mixture [27]. The mechanical properties of the cohesive elements can be determined from the

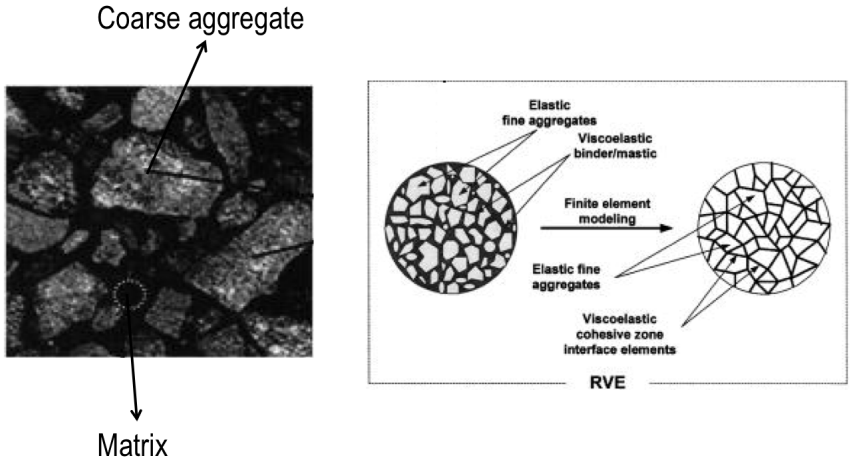

Figure 2.2: A typical asphalt concrete mixture is displayed with its finite element model representation [27].

standard fracture tests in the laboratory. Compared to the smeared FE model, the CZM model is far more efficient since the majority of the structure is modeled by elastic elements. Clearly the main drawback of the CZM is that the crack paths need to pre-determined in order to locate the cohesive elements. The CZM has been utilized to model the crack associated fracture damage in asphalt mixtures and can predict its performance under both nonlinear viscoelastic and fracture [28] . One study also utilized the CZM to investigate asphalts behavior due to fracture damage from repeated heavy truckloads [34].

Another continuum approach, which has recently attracted substantial attention, is the phase-field method. This method uses a parameter to describe the diffused damage around a discrete macro-crack, in which an intrinsic length scale is involved. The formulation of the method was anchored by the minimization of the potential energy of the structure, which leads to an efficient computation of fracture behavior. While classical fracture mechanics has been widely used to analyze initiation and propagation of cracks in asphalt, the phase field method has been more recently introduced for analyzing fracture dynamics. This method was used as a computational tool for analyzing Mode I cracking failure in asphalt binder using an energy-based formulation [34]. However, the existing formulation of the phase-field method was largely developed for linear elastic

systems [35, 36], which has a limited applicability to asphalt mixtures.

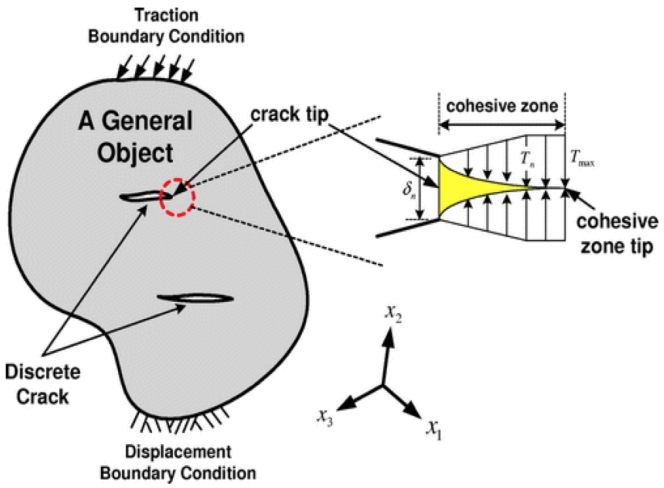

Figure 2.3: Schematic representation of cohesive zone concept for Mode-I fracture [37].

2.2.2 Discrete Element Modeling

As mentioned earlier, the continuum approach has its advantages for simplifying the analysis of asphalt mixtures through a smeared approach. By contrast, the discrete element model is designed to capture the details of the microstructure of the material. The model creates a more realistic alternative by taking into account the various size distributions of the aggregates [37]. In the proposed research, we plan to model the aggregates of the asphalt as particles and the GNP binders will be modeled by the bonds between particles. Figure 2.4 demonstrates a representation of the individual aggregates and the corresponding bonds [38]. The particle size can be determined directly from the size distribution of the aggregates while the behaviors of the particles are assumed to follow linear elasticity and a damage model is used to represent the behavior of the binders. This allows us to analyze the fracture behavior of the GNP-reinforced asphalt mixtures.

The discrete element model was pioneered by Cundall and Strack in the 1970s for simulating the behavior of large rock masses [39] . It has recently been applied to

rock mechanics to simulate the tool-rock interaction process (cutting or indentation of rock depending on direction of the cut). The model was further extended to concrete materials [37, 40, 41, 42]. In this analysis the rock was looked at as an assembly of particle that have the ability to displace and change independently from one another [29]. This allows the DEM to model damage and brittle fracture of the bonds due to the particles ability to move independently of each other [37]. Similar to the analysis of asphalt mixtures, an understanding of the relationship between the large-scale solid material and the smaller scale group of aggregates is necessary in order to utilize the DEM.

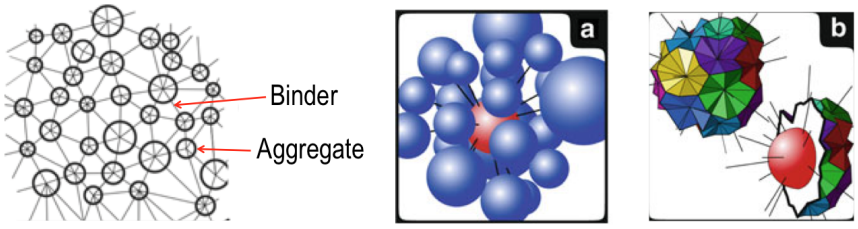

Figure 2.4: DEM representation of asphalt mixtures.

In the recent years, there has been a considerable amount of interests in applying discrete element models to asphalt mixtures [43, 44]. Studies have shown that, compared to the continuum-based finite element models, the discrete models could more realistically capture the underlying physics of the failure mechanism by explicitly taking into account the size distribution of the aggregates. One of the main obstacles of the use of discrete element model is the excessive computational time especially if one wants to explicitly represent fine aggregates. Meanwhile, the mechanical properties of the bonds are usually calibrated to fit some experiments on the mixture specimens [43]. Significant effort is required to accurately represent the microstructure of the mixture by utilizing image processing techniques[43, 44]. Although these models capture the microstructure of asphalt mixtures by explicitly modeling the aggregates, binder and interface as clumps particles with unique parameters, these models require many material properties [43]. There is a very limited amount of investigations on physically

determining the mechanical behavior of these bond contacts [44]. In addition, such detailed modeling of the asphalt mixture structure requires significant computational time.

It is evident that the continuum-based finite element model is not suitable for the aforementioned purpose because the constitutive model must be calibrated for the entire mixture. Although more efficient than smeared FE models, methods like the cohesive zone model has been utilized to model the crack associated fracture damage in asphalt mixtures and can predict its performance under both nonlinear viscoelastic and fracture, these models require a pre-determined crack path in order to locate the cohesive elements [45]. By contrast, discrete computational models fit well for the above-mentioned predictions since they model the aggregates and binders separately. One essential feature of the discrete element model is that it involves some characteristic length (e.g. particle size), which acts as a localization limiter regularizing the fracture energy.

Chapter 3

Discrete Computational Model

Chapter 3 presents the DEM computational model used in this research. Chapter 3.1 describes the model and behavior of the bonded particles. Chapter 3.2 discusses the mixture material parameters that are used in the program and Chapter 3.3 presents the input parameters for the bond material properties.

3.1 Model Description

In this study, we adopt a commercially available discrete element software (PFC3D) [46]. The PFC3D model was developed based on the bonded-particle model (BPM) introduced by Potyondy and Cundall (2004). The model was initially used for simulation of the behavior of rock, which can be considered as a cemented granular material with varying shaped grains. The BPM has been used as a reliable computational tool to explore the micromechanics that produces macroscopic behaviors, and to predict the macroscopic behaviors of the rock.

The BPM allows for finite displacements and rotations of discrete bodies, simulating the mechanical behavior of bonded non-uniform sized spherical rigid particles [47]. The rigid particles interact at soft contacts which possess finite normal and shear stiffnesses and the mechanical behavior is described by the force and moment at each contact due to the movement of the particles. When the bond between particles is formed, the force and moment are initialed to zero. As external forces are applied, Newton's

second law is used to determine the rotation and translation of the particles. The force-displacment law updates the contact forces that come from the relative motion of each particle at its contact point. The dynamic behavior of the model is handled by a time-stepping algorithm where the time step is so small that disturbances would not spread farther than to the particle immediately next to it. To realistically capture the dynamic behavior, a damping force is applied to each particle in order to consider the dissipation of kinetic energy [47].

In this study, we divide the aggregates into two categories, namely coarse aggregates and fine aggregates. For the particular mix design studied here, these two aggregate categories are separated at the aggregate size of 2.36 mm. When modeling the asphalt mixture in PFC3D, we consider only the coarse aggregates as discrete spheres whereas the bonds between these spheres represent the mixture of asphalt binder and fine aggregates (i.e. FAM). In such a way, we can effectively reduce the required computational time, which is one of the main obstacles in the application of discrete element models. The aggregates are modeled as sphere shaped particles which is assumed to be a realistic representation of the angular aggregates in the asphalt mixtures. In the model, the spherical particles are modeled as rigid bodies, and the bonds between these rigid particles are responsible for transmitting both force and moment, which resist the relative motion of the spheres.

The inter-particle bond is similar to a set of elastic springs that are uniformly distributed over the cross section on the contact plane (Figure 3.1). The elastic behavior of the bond between the particles contains a total force and moment relating to the normal and shear components with respect to the contact plane. At each contact surface, the force and moment can be expressed as

$$\vec{F} = F_n\vec{n} + F_s\vec{t} \tag{3.1}$$

$$\vec{M} = M_n\vec{n} + M_s\vec{t} \tag{3.2}$$

where F_n and M_n are the force and moment components in the normal direction, respectively, and F_s and M_s are the force and moment components in the shear direction, respectively (Figure 3.1). During each time increment of the simulation, the change of these force and moment components are further related to the relative motion of the particles as follows:

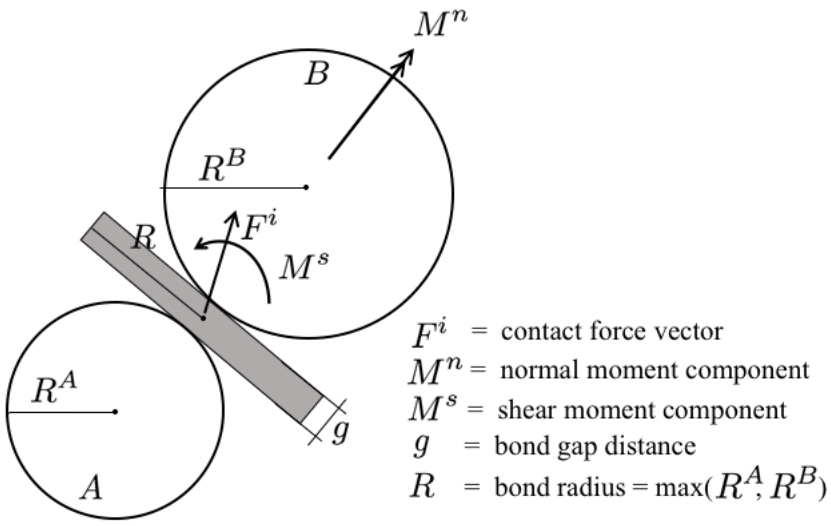

Figure 3.1: Linear elastic behavior of bond for a) normal, and b) shear force. Bond gap and bond radius dimensions are shown

$$\Delta F_n = k_n A \Delta \delta_n \tag{3.3}$$

$$\Delta F_s = -k_s A \Delta \delta_s \tag{3.4}$$

$$\Delta M_n = k_n J \Delta \theta_n \tag{3.5}$$

$$\Delta M_s = -k_s I \Delta \theta_s \tag{3.6}$$

where A, I, and J are the area, moment of inertia, and polar moment of inertia of the bond, respectively. Based on the calculated force and moment, we can determine the maximum normal and shear stresses in the bond based on elastic analysis, i.e.:

$$\sigma_{max} = -F_n/A + |M_s|\bar{R}/I \tag{3.7}$$

$$\tau_{max} = F_s/A + |M_n|\bar{R}/J \tag{3.8}$$

where $\bar{R}$ is the bond radius, which is set to equal to the maximum radius of the two particles. As the maximum shear stress exceeds the strength limit, the bond breaks and the force is equal to zero. As the maximum tensile stress exceeds the strength limit, the bond exhibits softening and the force decreases linearly as the bond length

increases until the force is equal to zero. When the force reaches zero, the bond is broken and loses its load-carrying capacity, which indicates that a discrete crack was formed between these two particles. Figure 3.3 shows the constitutive relation of the bond under pure tension, in which T_n a denote the tensile strength of the bond and α is the coefficient of the decreasing slope multiplied by the normal stiffness that produces the required fracture energy of the bond. The fracture energy of the bond is equal to the work of fracture divided by the cross sectional area. Bond fracture energy is a function of the young's modulus and tensile strength and can be calculated as:

$$G_{f,bond} = \frac{W}{A} = \frac{\sigma_{max}^2 L}{2E}(1 + \frac{1}{\alpha}) \tag{3.9}$$

where α is the coefficient of the softening portion of the slope for the constitutive behavior of the bond and $E = k_n L$ and L is the bond length and is set equal to 1 mm which is a reasonable assumption because the average diameter of the particles in FAM is approximately 1 mm. Figure 3.2 shows a 3-D representation of the bond between two particles and indicates the bond length and cross sectional area.

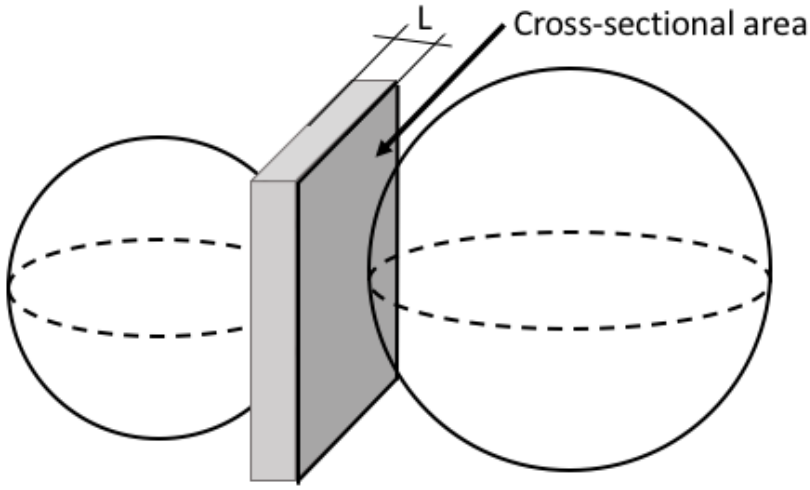

Figure 3.2: Three-dimensional representation of the bond between two particles. The cross sectional area and bond length are indicated.

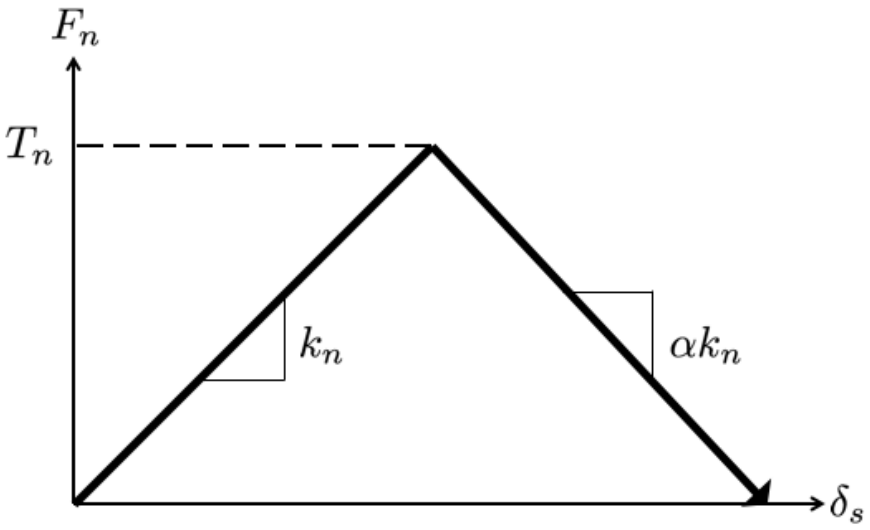

Figure 3.3: Linear parallel-bond model behavior with softening

3.2 Input of Mixture Parameters

The main advantage of the discrete element model is its capability of capturing the details of the microstructures. The present model requires the input of geometry and mixture material properties that include the particle size distribution, the porosity of the particles, the bond gap and radius of the bond. The particle size distribution can be obtained based on the known aggregate size distribution. Note that in this study we only explicitly consider coarse aggregates whereas the fine aggregates are lumped with the binder. For the particular mix design studied, the diameter of the coarse aggregates varies from 2.36 mm to 9.5 mm. The distribution of the particles follows that of the asphalt mixture with various percentages passing through each sieve. To implement the size distribution information into PFC3D, we determine the particle size intervals for equal intervals of the passing rate (Figure 3.4), from which we generate a smooth particle distribution curve. This is similar to the Latin Hybercube Sampling technique for stochastic simulations [48].

The ratio of void space to the total volume of the larger aggregates that are modeled

in the simulation must also be considered. The value assigned to the porosity takes into account the air voids in the entire asphalt mixture as well as the volume occupied by the binder and fine aggregates. The mix design consists of 48% coarse aggregates, 52% fine aggregates, 5.5% binder and 3-7% air voids. A porosity of 40% is assumed to be a reasonable value for capturing the behavior of the asphalt mixture.

The parallel bond installation gap and bond radius are shown in Figure 3.1. The gap was determined to be 0.05 mm. This value was chosen so that all particles were bonded to their immediate neighboring particles to simulate aggregates that are completely coated in asphalt binder. The bond radius is equal to the maximum radius of the two particles in contact, which was chosen to model the asphalt binder that surrounds the entire aggregate in the compacted mixture.

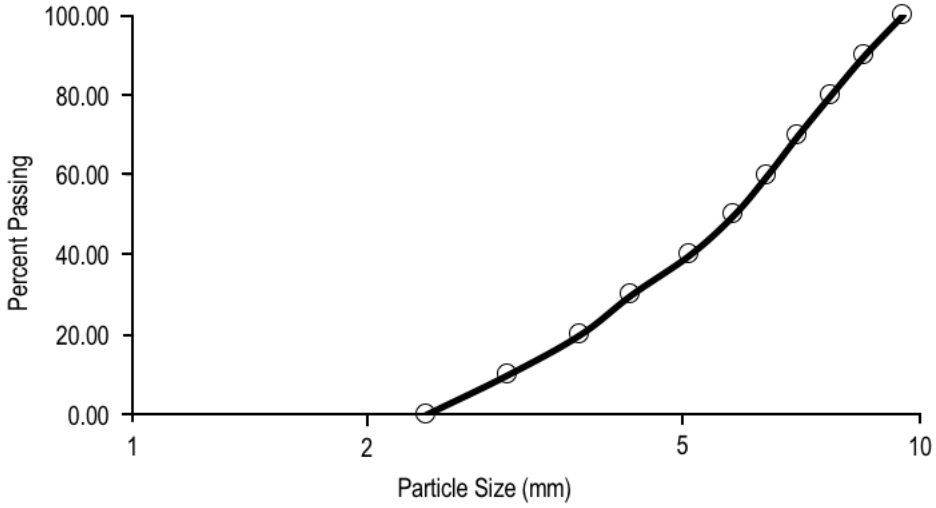

Figure 3.4: Particle distribution curve for coarse aggregates

Based on the aforementioned geometrical parameters, the PFC3D code is used to generate a SCB specimen with a diameter of 150 mm and a thickness of 25 mm, which is used for the experimental investigation. The specimen contains a crack of 3 mm in width and 20 mm in length at the middle of the bottom surface. The SCB specimen is simply supported with a span of 120 mm and is loaded on the top. Figure 3.5 shows one realization of the geometry of the specimen.

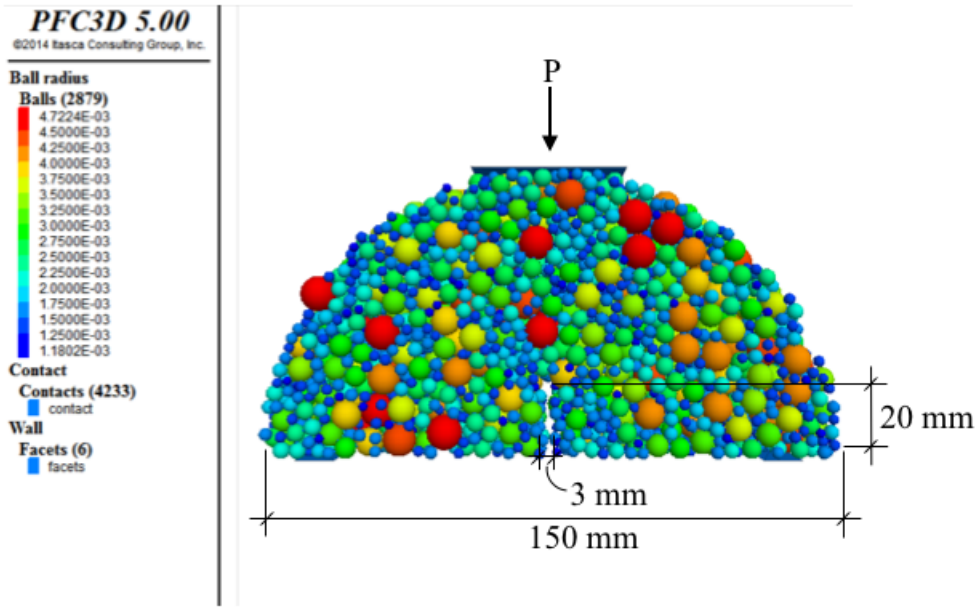

Figure 3.5: Discrete element modeling of semi-circular bend specimen (Ball radius dimensions are shown in meters)

3.3 Input of Bond Material Parameters

In addition to geometrical parameters, the PFC3D requires six material parameters, which describe the behavior of the bond contact. These parameters include the Young modulus, the Poisson ratio, the tensile strength, the bond fracture energy, the shear strength, and the frictional angle. These parameters are determined as follows:

1. The Young modulus and the tensile strength of the bond are determined from the BBR test [49]. The Young modulus is directly inputted into the model while the tensile strength is scaled due to the size effect discussed in the later section. The test is conducted on compacted samples of asphalt binder and fine aggregates. The fine aggregates used in the FAM had a diameter less than 2.36 mm. The details of the experiments on FAM will be described in the next section.

2. The Poisson ratio varies little at low temperatures, therefore it is taken to be considered a constant value, assumed to be 0.3. The stiffness ratio of the bonds,

the normal stiffness divided by the shear stiffness, is calculated from the Poisson ratio where:

$$k^* = \frac{k_n}{k_s} = \frac{E}{G} = 2(1+\nu) \tag{3.10}$$

3. Shear strength is used to model the slip behavior of the bond, which can be considered as mode II fracture. In the simulation of SCB tests, the asphalt mixture primarily experiences tensile cracking (mode I fracture). Therefore, we set a relatively high value of shear strength (20 MPa) so that the bond will primarily fail in tension

4. Friction angle is important if the specimen experiences compressive failure. This is certainly not the case for SCB specimens. Since the simulation of the SCB test primarily experiences tensile cracking, the friction angle has no effect on the simulation.

5. The fracture energy of the bond is used to determine the slope of the softening part of the linear parallel-bond model behavior. The fracture energy of the bond is the area under the force-displacement curve of the bond divided by the area of the bond. The bond fracture energy is used as a fitting parameter to match the post-peak behavior of the simulation to the experimental results.

Parameter	Input
Porosity	0.4
Bond Gap	0.05 (mm)
Bond Radius	Max(R^1, R^2)
Poisson Ratio	0.3
Bond Fracture Energy	12.64 (J/m^2)
Elastic Modulus	4.29 (GPa)
Tensile Strength	7.05 (MPa)
Cohesion	20 (MPa)
Friction Angle	40°

Table 3.1: Input parameters for PFC3D.

Table 3.1 lists both the geometrical properties, mixture material properties, and bond material parameters that are inputted into the PFC3D for the simulations of SCB experiments with unmodified asphalt binder. Table 3.2 lists the material properties of

Type of GNP	850			4827		
Amount of GNP added	0.5%	1%	3%	0.5%	1%	3%
Tensile Strength (MPa)	9.07	8.27	10.05	10.40	10.26	10.47
Elastic Modulus (GPa)	3.87	3.87	4.52	4.81	4.76	3.74
Bond Fracture Energy (J/m^2)	22.18	18.55	23.19	23.60	22.95	30.59

Table 3.2: Material input parameters for binder modified with various amounts of GNP.

tensile strength, elastic modulus and bond fracture energy for the simulations with various amount and types of GNP. The rest of the parameters in Table 3.1 were unchanged. These parameters are discussed further in Chapter 4. The influence of these parameters on the simulated behavior will be presented in Chapter 5.2.

Chapter 4

Experimental Investigation

Chapter 4 discussing the procedures and results for the BBR and SCB experiments performed in this research. Chapter 4.1 discusses the preparation of the specimen for testing. Chapter 4.2 presents the mixing technique used to mix the GNP and asphalt binder and discusses the benefits of this method. Chapter 4.3 presents the procedure and results from the BBR tests performed on FAM with various amounts of GNP added. Finally, Chapter 4.4 discusses the procedure and results from performing the SCB test on asphalt mixtures with various amounts of GNP added.

4.1 Description of Materials and Preparation of Specimens

In this study, asphalt mixtures of both modified and unmodified asphalt binder are tested. The unmodified asphalt binder PG 58-34 was used and obtained from Minnesota Department of Transportation (MnDOT), and manufactured by Flint Hills Resources. The binder was heated for 30 minutes in an oven at $150°C$. The binder was then short term aged using a rolling thin film oven (RTFO) in accordance with the AASHTO standard method T240. After short-term aging, a pressurized aging vessel (PAV) was used to accelerate the aging of the mix. This was in accordance with AASHTO Standard method R28-09 and simulates the in-service oxidative aging in the field for an asphalt pavement during 5-7 years of service. After the aging process was finished, the blend was degassed using a vacuum oven and was stored in small cans and reheated to prepare

BBR and SCB test samples.

The modified binder samples contained various amounts of Graphite Nanoplatelets (GNP). Recent studies have shown that the GNP can be easily incorporated into asphalt binders, and due to its relatively low aspect ratio, less potential clustering is observed during the mixing when compared to other nanomaterials. Strength tests showed that GNP modified asphalt binders exhibit superior flexural strength at low tempatures compared to conventional binders. Two different types of GNP were used, 4827 and 850 where type 4827 represents true GNP powder and type 850 is a less expensive GNP flake. The added amount of GNP was 0.5%, 1% and 3% by weight of binder for the modified asphalt binders.

The samples for the SCB experiments followed the mix design provided by the MnDOT. The mixture was prepared using Superpave mix design. The details of the mix design groups are as follows: The mix design is composed of 5.5% binder and three different types of aggregates including, 42% SSG sand, 25% Kraemer 3/8 minus (limestone), and 30% Kraemer 3/8 chip (limestone). The mix design can be found in table A.1. The compaction was performed using a Brovold Gyratory Compactor. The number of gyrations performed were 60 gyrations. The bulk specific gravity (Gmb) and the maximum specific gravity (Gmm) for the mixture were determined. An air void content of 7.7% was achieved for the compacted specimen.

4.2 Mixing of GNP into Asphalt Binder

The technique used to mix the GNP into the asphalt binder was an advanced method that utilized a high shear mixing device. Compared to previous results where the GNP was mixed into the asphalt by hand using a stirring technique, higher flexural strengths and more desirable behaviors are exhibited when the asphalt is mixed with the high shear mixing device. This mixing technique is more effective at dispersing the GNP into the asphalt binder. A common method for measuring dispersion of nanomaterials through materials is the SEM techniques. However, this is not a useful tool for measuring the dispersion of the GNP into the asphalt binder since both the binder and GNP are the same color. Conductivity tests were performed on samples of binder with various amounts of GNP in order to measure the dispersion of the GNP in the asphalt binder.

A four probe conductivity test was performed on binder samples with various amounts of GNP. Experiments were performed on unmodified samples and samples with 3% and 6% for both types of GNP, 4827 and 850. The samples were prepared using the high shear mixing device to mix the asphalt and binder. The binder was then poured into molds with dimensions of 6.35 mm thick by 12.70 mm wide and 127 mm long. The four point probe and test equipment is used to determine the conductivity of the samples. Two of the probes are used to measure voltage and two of the probes are used to source current. Four probes are spread out along the sample such that there is an equal distance of material between each probe and the probe set up can be seen in Figure 4.1. The outside probes source the current while the two inside probes sense the voltage drop across the sample. The power supply was 1 volt and the current was 0.0001 micro Amps. Three tests were performed on samples with a given amount and type of GNP.

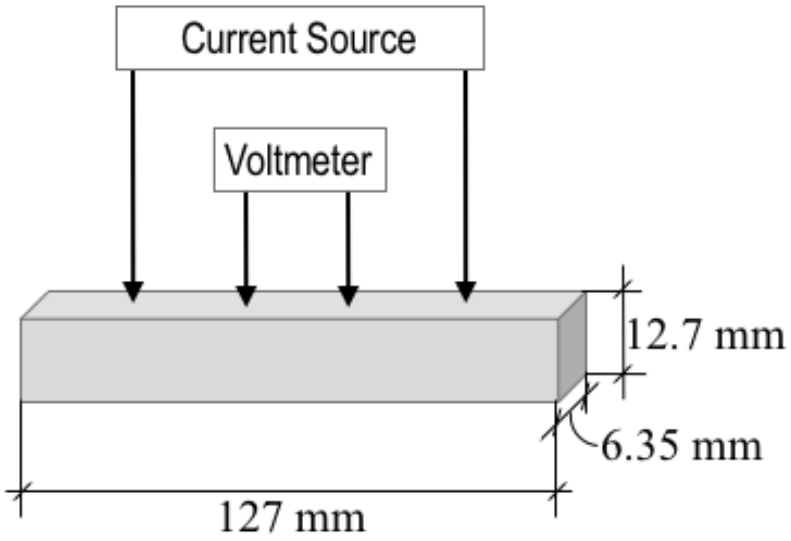

Figure 4.1: Four-point probe setup

The results in Table 4.1 indicate that voltage is measured between the inner probes

GNP Type			4827			
Amount of GNP		3%			6%	
Sample	1	2	3	1	2	3
Voltage, (mV)	3	2.6	3	4	2	3
GNP Type			850			
Amount of GNP		3%			6%	
Sample	1	2	3	1	2	3
Voltage, (mV)	2.5	4	3	3.5	4	4

Table 4.1: Voltage results from conductivity test on samples of binder with GNP.

for the binder samples that contain GNP while no voltage is measured across the unmodified sample. The voltage measured for the samples with various amounts of GNP ranged from 2-4 mV.

When the same conductivity test was performed on samples of binder mixed with GNP by hand and not using the high shear mixing method, no voltage was measured for any of the samples including the samples with 3% or 6% of GNP. When the conventional mixing procedure was used, no and no conductivity was observed, therefore the high shear mixing technique is more effective at dispersing the GNP throughout the binder and is the preferred method for achieving desirable flexural strengths and behavior.

4.3 Bending Beam Rheometer Test on Fine Aggregate Mixture Specimens

In order to determine the tensile strength and the Young Modulus of the FAM, specimens were prepared for the BBR test. The FAM consists of the fines portion of the mixture with aggregates passing through the No. 8 sieve (2.36 mm). The ignition oven test (AASHTO T308) is used to determine the binder content within the fine aggregate portion of the full mixture [50]. The full mixture requires 5.5% binder, using PG 58-34 binder. The percent binder within the fine aggregate mixture was determined to be 8.7%. This was determined by establishing the aggregate batch size that would be used for the FAM sample and preparing a loose sample of the total mixture. The samples were conditioned for a 2-h period at 135$^{\circ}C$. The mixture was passed throw a No. 8 sieve and the parties passing through were oven dried at a temperature of 110C. The

mass of the materials of each group were recorded. The pan was placed in an ignition oven to bur the asphalt in accordance with AASHTO T 308. After the binder burning is complete the mass of the pan with materials was recorded. The percent binder was calculated as follows:

$$P_b = \frac{W_M - W_A}{W_M - W_P} \times 100 \tag{4.1}$$

where W_M, W_A, and W_P are the weight of the mixture in pan, materials after binder burning and weight of the pan, respectively.

The BBR test was performed according to [49]. The BBR test system consists of a test frame, a controlled temperature environment, and a computer controlled automated data acquisition component. The sample supports are 3.0 mm in top radius and are at an angle of 45 degrees with the horizontal axis. The supports are made of stainless steel and placed 102.0 mm apart. The width of the supporting strips is 9.5 mm. The supports also include vertical alignment pins that are 2 to 4 mm in dimeter and are placed at the back of each sample support at 6.75 mm from the center of the support. A blunt-nosed loading shaft with a spherical contact point of 6.35 mm radius is used. A load cell with a minimum capacity of 9.806 mN and having a minimum resolution of 2.5 mN is mounted in-line with the loading shaft to measure contact and test load. A linear variable differential transducer is mounted axially above the loading shaft capable of resolving a linear movement less than 0.15 micrometers with a range of at least 6 mm is used to measure the deflection of the test beam.

The FAM was compacted with the same gyratory compactor following the mixture preparation procedure described in the proposed standard test method for preparing dynamic mechanical analyzer specimen [50]. Compacted cylinders of the fine aggregates and binder were prepared and samples were then cut to the dimension of 6.35 mm thick by 12.70 mm wide and 127 mm long. FAM specimens were obtained for unmodified GNP and for each type and percentage of GNP for a total of 7 different FAM. The thickness and width of each beam were measured in three places and the average was reported for calculation purposes. The BBR strength test was performed on three of each of the FAM specimens at T $=24°C$, from which the load-deflection curve was recorded. The test was performed by applying a load of 44 N in 150 seconds. The load-deflection curves for the first sample of unmodified binder are shown in Figure 4.2.

From these plots the maximum load applied and load and the deflection at 50% of the maximum load are obtained. These values are used to calculate the tensile strength and modulus as follows:

$$E = \frac{PL^3}{4bh^3\delta} \tag{4.2}$$

$$\sigma = \frac{3P_mL}{2bh^2} \tag{4.3}$$

where P_m is the maximum load capacity, L, b, h are the length, width and height of the specimen, respectively, and is the deflection at which the maximum load is reached. The average tensile strength and modulus were obtained from the three tests on each of the seven FAM. The calculated results for tensile strength and modulus are shown in Table 4.2. The tensile strength for FAM modified with various amounts of GNP show a significant increase of approximately 26% to 42% compared to unmodified FAM. The values obtained for the young's modulus vary from 3.74 GPa to 4.81 GPa.

Type of GNP			850			4827	
Amount of GNP added	0%	0.5%	1%	3%	0.5%	1%	3%
Tensile Strength (MPa)	6.07	9.07	8.27	10.05	10.40	10.26	10.47
Elastic Modulus (GPa)	4.29	3.87	3.87	4.52	4.81	4.76	3.74

Table 4.2: Nominal tensile strength and elastic modulus of FAM for unmodified and modified binder

It should be emphasized that nominal tensile strength calculated from the BBR test does not represent the true tensile strength of the material due to the size effect in quasibrittle fracture. Since it is well known that asphalt mixtures can be considered as a quasibrittle material at low temperatures [55, 56, 57, 58], it is expected that the nominal tensile strength would be subjected to a size effect. By contrast, the value of the Young modulus obtained from the BBR test can directly be inputted into the PFC3D since size effect is absent in elasticity [59].

To determine the actual tensile strength of the material, we note that, for geometrically similar beams, the size effect on the nominal tensile strength can be approximated as

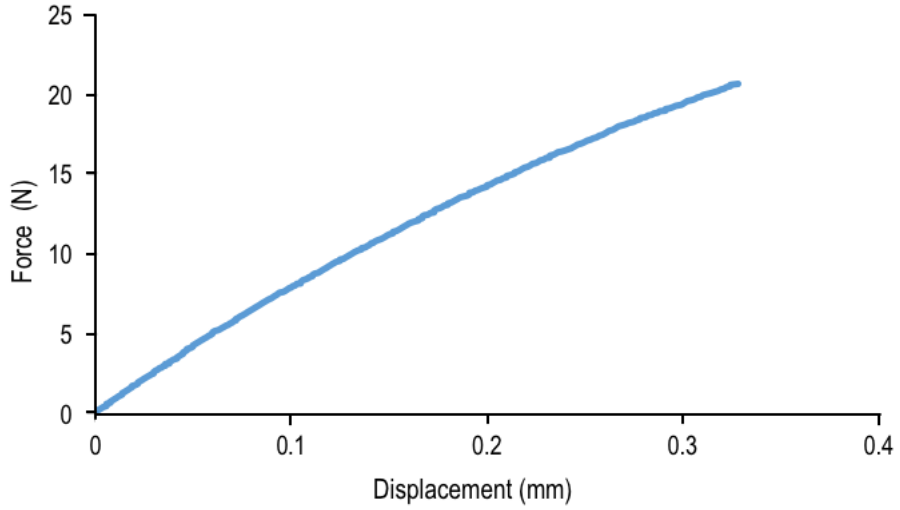

Figure 4.2: Load vs. time and deflection vs. time curves of the BBR test for sample 1

$$\sigma_N = T_n[C_1 D_b/D + (C_2 D_b/D)^{2r/m}]^{1/r} \tag{4.4}$$

where C_1, C_2, r are constants depending the specimen geometry, m is the Weibull modulus and D_b is the thickness of the boundary layer, which is about four times the average aggregate size [59]. Previous studies have determined the size effect curve represented by Equation 4.4 for three-point bending of concrete specimen (Figure 4.3). The Weibull modulus of asphalt mixtures is very close to that of concrete [58]. Therefore, we can use Figure 4.3 to determine the ratio between the nominal tensile strength and the actual material tensile strength for any given value of D/D_b. In this study, D_b is about 1 mm (average aggregate size is about 0.25 mm) and the depth D_0 of BBR beams is 6.07 mm. Based on Figure 4.3, we have $\sigma_N(D_0) \approx 0.85T_n$ or $T_n \approx 7.05$ MPa. Table 4.3 shows all the values of strength after scaling that are inputted into the model.

Type of GNP			850			4827	
Amount of GNP added	0%	0.5%	1%	3%	0.5%	1%	3%
BBR Tensile Strength (MPa)	6.07	9.07	8.27	10.05	10.40	10.26	10.47
Scaled Tensile Strength (MPa)	7.05	10.53	9.60	12.19	12.08	11.92	12.16

Table 4.3: Nominal tensile strength of FAM for unmodified and modified binder after scaling

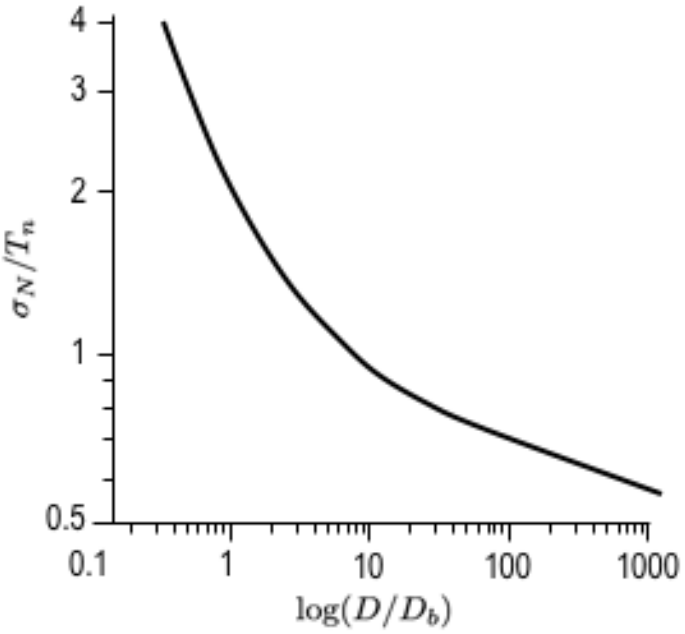

Figure 4.3: Size effect curve for three-point bending of concrete specimen

4.4 Semi-Circular Beam Tests

In order to investigate the fracture behavior of the asphalt mixtures, we performed the SCB test following AASHTO TP-105 and the measured load-deflection curve is compared with the simulation by the PFC3D code. The SCB test method takes advantage of the simple specimen preparation from Superpave Gyratory compacted cylinders and the simple loading setup [60]. Figure 4.4 shows the set-up of SCB tests.

In this study, a MTS servo-hydraulic testing system equipped with an environmental chamber was used to perform the SCB test. The SCB samples were symmetrically supported by two fixed rollers and had a span of 120 mm. The load line displacement (LLD) was measured using a vertically mounted Epsilon extensometer with 38 mm gage

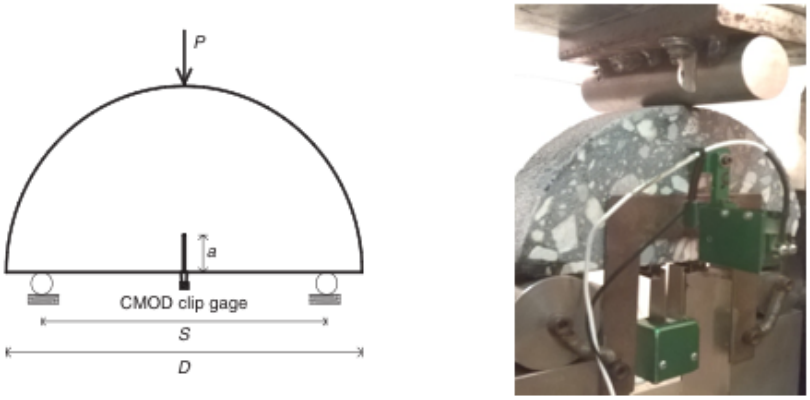

Figure 4.4: Set-up of SCB Tests

length and ±1 mm range; one end was mounted on a button that was permanently fixed on a specially made frame, and the other end was attached to a metal button glued to the sample. The CMOD was recorded by an Epsilon clip gage with 10 mm gage length and a +2.5 and -1 mm range. The clip gage was attached at the bottom of the specimen. Considering the brittle behavior of asphalt mixtures at low temperatures, the CMOD signal was used as the control signal to maintain the test stability in the post-peak region of the test. A constant CMOD rate of 0.0005mm/s was used and the load and load-point displacement (P-u) curve was plotted. A contact load with maximum load magnitude of 0.3 kN was applied before the actual loading to ensure uniform contact between the loading plate and the specimen. The testing was stopped when the load dropped to 0.5 kN in the post peak region. All tests were performed inside an environmental chamber. Liquid nitrogen was used to obtain the required low temperature. The temperature was controlled by the environmental chamber temperature controller and verified using an independent platinum RTD thermometer. The SCB tests were performed at T = $24°C$.

Figure 4.5 presents the load-deflection curve averaging the measurements of five specimens for unmodified asphalt binder and binder modified by various amounts of 850

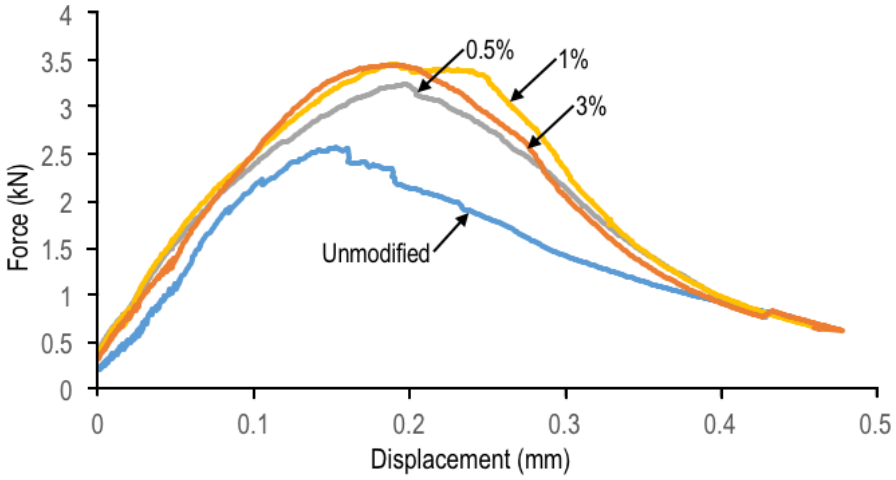

Figure 4.5: Load-deflection curve for asphalt mixtures with unmodified binder and various amounts of GNP 850

GNP. Figure 4.6 presents the average load-deflection curve for mixtures with unmodified binder and GNP 4827. It is clear that the specimens exhibit a gradual softening behavior due to the propagation of the macrocrack, which signifies that the material behaves in a quasibrittle manner. The fracture energy of the asphalt mixture was calculated for the unmodified asphalt binder and the binder modified by GNP and can be found in Table 4.4. According to [54], the fracture energy (G_f) is calculated as the work of fracture divided by the ligament area:

$$G_f = \frac{W_f}{A_{lig}} = \frac{\int P du}{(r-a)t} \tag{4.5}$$

where W_f is the work of fracture, calculated as the area under the force-displacement curve in Figure 4.5 and Figure 4.6 and A_{lig} is the ligament area. The ligament area is calculated as the distance between the tip of the notch and the bottom of the specimen multiplied by the thickness. The fracture energy of GNP modified asphalt mixtures is significantly greater than the unmodified binder mixtures, ranging from an increase of approximately 18% to 27%. The peak load capacity of the asphalt mixtures also show a significant increase for asphalt binder modified with GNP compared to unmodified binder with a percent increase of approximately 18% to 26%. These results indicate

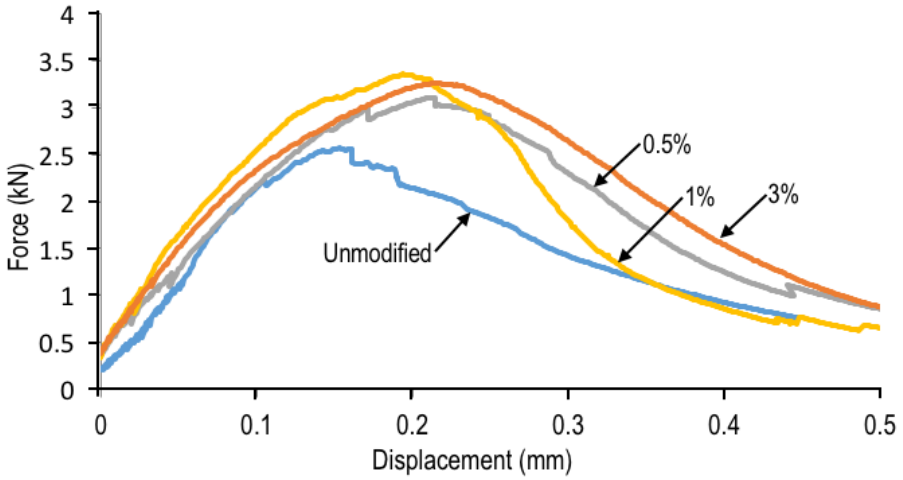

Figure 4.6: Load-deflection curve for asphalt mixtures with unmodified binder and various amounts of GNP 4827

that GNP is very effective at improving the fracture behavior of asphalt mixtures at low temperatures.

Type of GNP			850			4827	
Amount of GNP	0%	0.5%	1%	3%	0.5%	1%	3%
Fracture Energy (J/m^2)	745.68	950.94	1008.74	942.92	1020.04	911.12	1113.68

Table 4.4: Fracture energy of the asphalt specimen from the SCB test

Chapter 5

Results and Discussion

Chapter 5.1 presents the discussion of the comparison between the simulation and experimental results. A parametric study is also presented in Chapter 5.2 exploring how the bond behavior would affect the overall mechanical response of the asphalt mixtures. The results of the parametric study can be used a design tool for asphalt pavements with various amounts of GNP. The required tensile strength of the pavement for target fracture behavior can be determined using the results from the parametric study. The design procedure is discussed in Chapter 5.3.

5.1 Comparison of DEM and Experimental Measurements

DEM simulations with various input parameters for the tensile strength, elastic modulus and bond fracture energy for asphalt mixtures with different amounts of GNP 4827 and GNP 850 were compared to the experimental measurements obtained from the SCB tests. Each experimental result is the average of five different tests performed on SCB specimens with each amount of GNP. The error is calculated as the standard deviation divided by the square root of the number of experiments. Generally, the elastic response and peak load are reasonably predicted using input parameters from experiments on FAM.

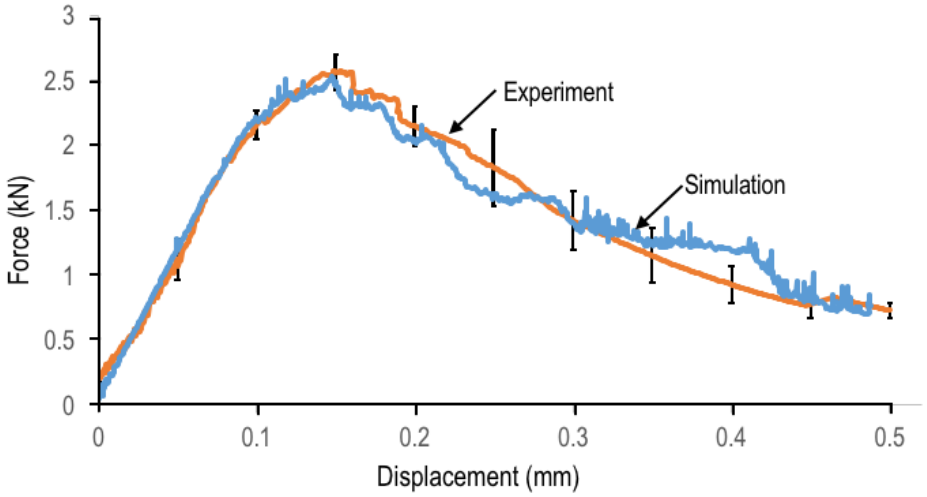

Figure 5.1: Load vs. Displacement plots for experimental results and PFC3D Model for unmodified binder.

Figure 5.1 displays the results for the SCB experimental measurements on unmodified asphalt mixtures and the DEM simulation for the input parameters obtained from BBR experiments on unmodified FAM. It is evident that the elastic response and peak load capacity predicted by the DEM model agree reasonably well with the experimental measurements. The simulation is able to predict the post-peak behavior using the bond fracture energy as a fitting parameter.

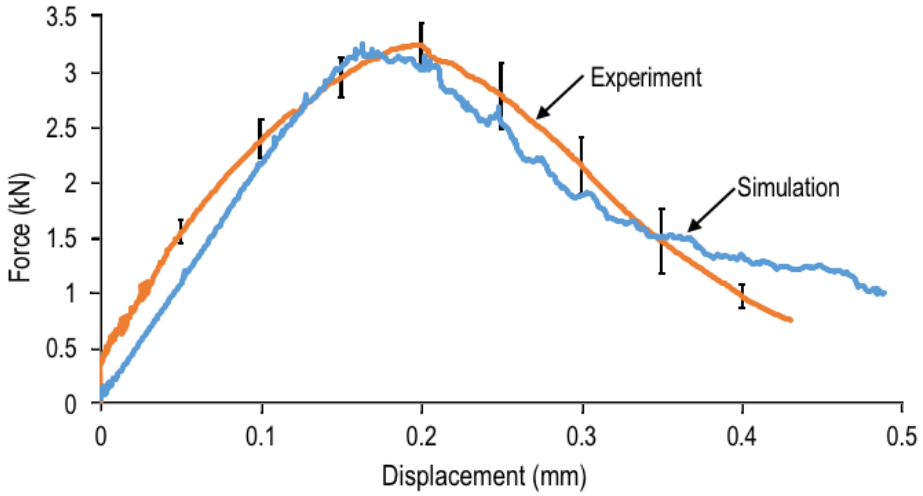

Figure 5.2: Load vs. Displacement plots for experimental results and PFC3D Model for binder with 0.5% GNP 850.

Figures 5.2 to 5.4 display the comparison between the experimental and simulations results for asphalt binder modified with GNP 850. Figure 5.2 compares the experimental and simulation results for asphalt mixtures modified with 0.5% GNP 850. The peak load capacity predicted from the DEM model is in agreement with the experimental results. The force-displacement curve for the simulation starts at the origin while the experimental results start at an initial value of force. This can be due to instances were data recording starts at a load value different from zero. Although the elastic response is not identical due to the initial loading, the displacement at which the peak load occurs in the simulation is in agreement with the experimental results. The post-peak behavior of the simulation shows a steeper decrease initially and then decreases more slowly than the experimental results. However, the area under the force-displacement curves are similar, producing similar results for the fracture energy.

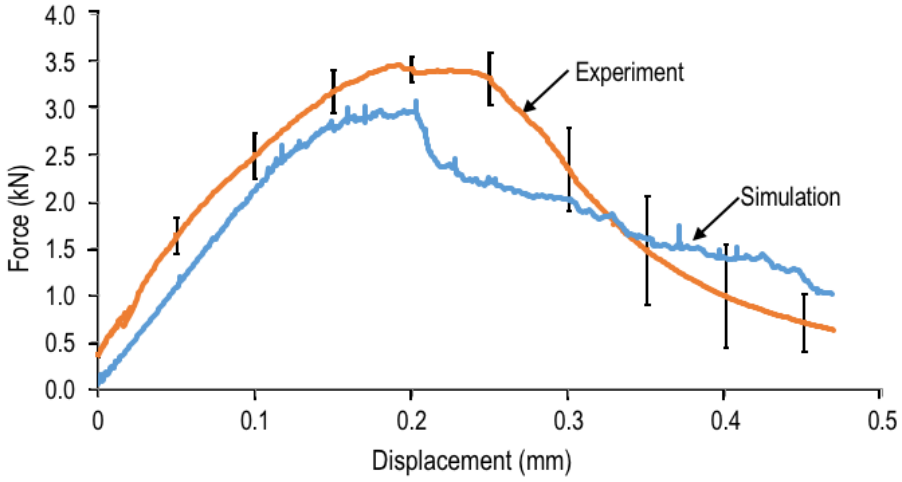

Figure 5.3: Load vs. Displacement plots for experimental results and PFC3D Model for binder with 1% GNP 850.

Figure 5.3 compares the simulation prediction and experimental results for asphalt mixtures with 1% of GNP 850. The simulation under-predicts the peak load capacity of the mixtures compared to the experimental results, even when size-effect is considered. The peak load capacity obtained from the experiment is approximately 16% higher than the peak-load capacity predicted in the simulation. Similar to the results for 0.5% GNP 850, the experimental results indicate that data recording starts at a load value that is different from zero while the simulation starts at the origin. Although the peak-load capacity of the simulation does not achieve as high of a capacity as the experimental results, the elastic response is in agreement. The post-peak behavior of the simulation displays a sharper decrease initially and then more gradually decreases then the experimental results.

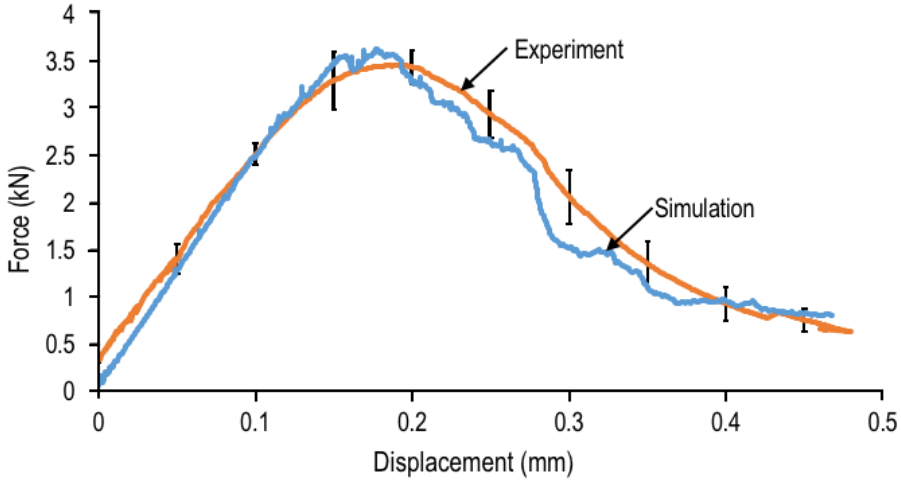

Figure 5.4: Load vs. Displacement plots for experimental results and PFC3D Model for binder with 3% GNP 850.

Figure 5.4 compares the simulation prediction and experimental results for asphalt mixtures with 3% of GNP 850. It is seen that the elastic response and the peak load capacity predicted by the simulation agree reasonably well with the experimental measurements. However, the data recording started at a load value greater than zero for the experiment while the simulation starts at the origin. The post-peak behavior predicted by the simulation is also in agreement with the experimental results, with a slightly steeper decreasing slope.

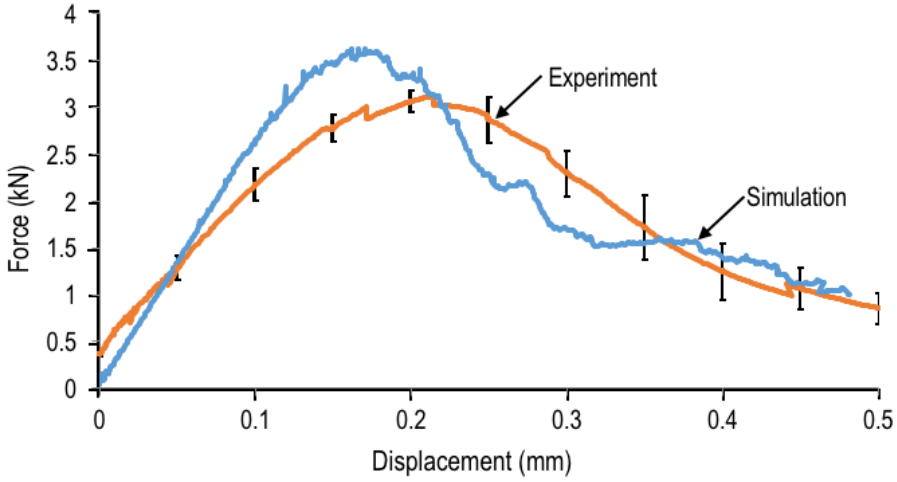

Figure 5.5: Load vs. Displacement plots for experimental results and PFC3D Model for binder with 0.5% GNP 4827.

Figures 5.5 to 5.7 display the comparison between the experimental and simulations results for asphalt binder modified with GNP 4827. Figure 5.5 compares the simulation prediction and experimental results for asphalt mixtures with 0.5% of GNP 4827. The peak load capacity of the mixture is over-predicted by the simulation by approximately 14%. The elastic behavior predicted by the simulation is more stiff than the experimental results and the experiment exhibits an initial loading while the simulation starts at the origin. The post-peak behavior predicted by the simulation is initially more steep but then converges with the experimental results.

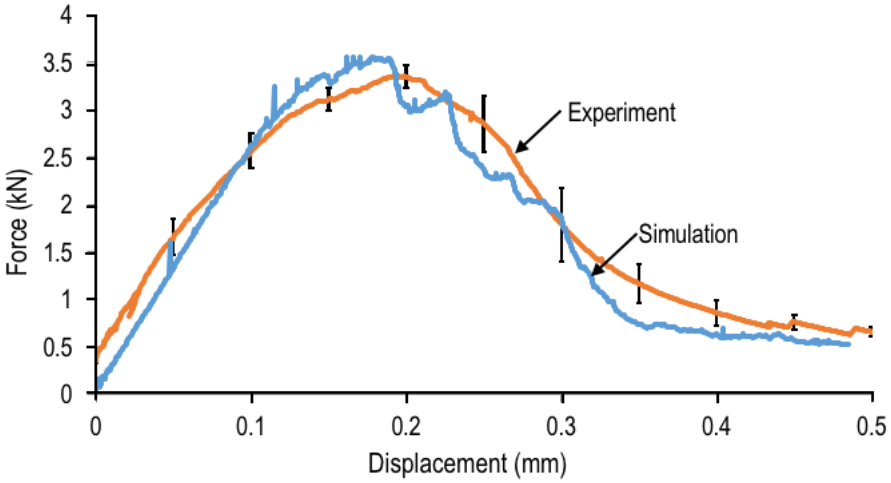

Figure 5.6: Load vs. Displacement plots for experimental results and PFC3D Model for binder with 1% GNP 4827.

Figure 5.6 compares the simulation prediction and experimental results for asphalt mixtures with 1% of GNP 4827. The peak load capacity predicted from the DEM model is in agreement with the experimental results. The force-displacement curve for the simulation starts at the origin while the experimental results start at an initial value of force. The simulation predicts a more steep post-peak behavior but then converges with the experimental results.

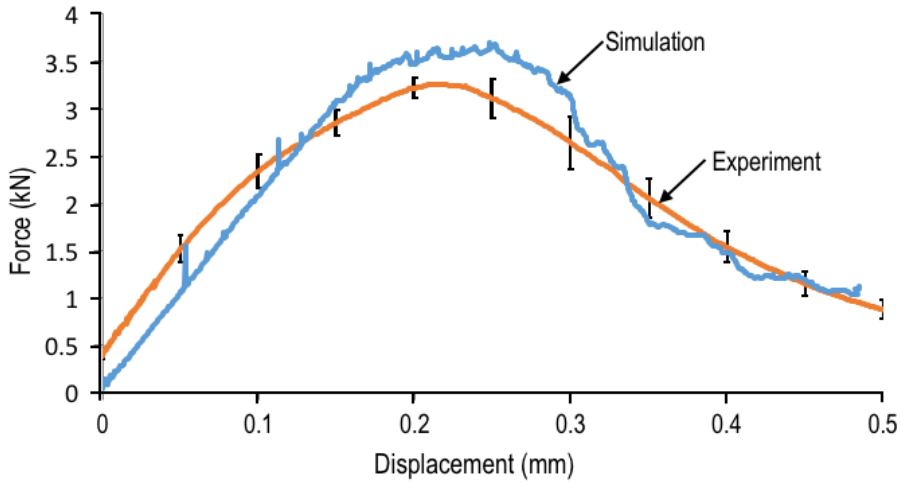

Figure 5.7: Load vs. Displacement plots for experimental results and PFC3D Model for binder with 3% GNP 4827.

Figure 5.7 compares the simulation prediction and experimental results for asphalt mixtures with 3% of GNP 4827. The peak load capacity of the mixture is over-predicted by the simulation by approximately 12%. The force-displacement curve for the simulation starts at the origin while the experimental results start at an initial value of force. The elastic response of the simulation predicts a similar displacement for where the peak load capacity is achieved when compared to the experimental results. The simulation initially predicts a more steep post-peak behavior but then converges with the experimental results.

From Figure 5.1 through Figure 5.7, it is seen that the elastic response and the peak load capacity predicted by the PFC3D model agree reasonably well with the experimental measurements. The comparison indicates that the direct use of the elastic response of the FAM is able to reasonably predict the elastic behavior of the mixtures, which implies that the elasticity of the mixtures is mainly governed by the FAM. Meanwhile, the PFC3D model is also able to predict the peak load. This indicates that the bond strength is a governing factor of the overall load capacity of the mixtures. The simulation is able to predict post-peak behavior with the input of the bond fracture energy. This parameter was not directly obtained from BBR tests on FAM, but is a function

of the Young's modulus and tensile strength and was used as a fitting parameters to match the experimental results of the mixture produced from the SCB tests.

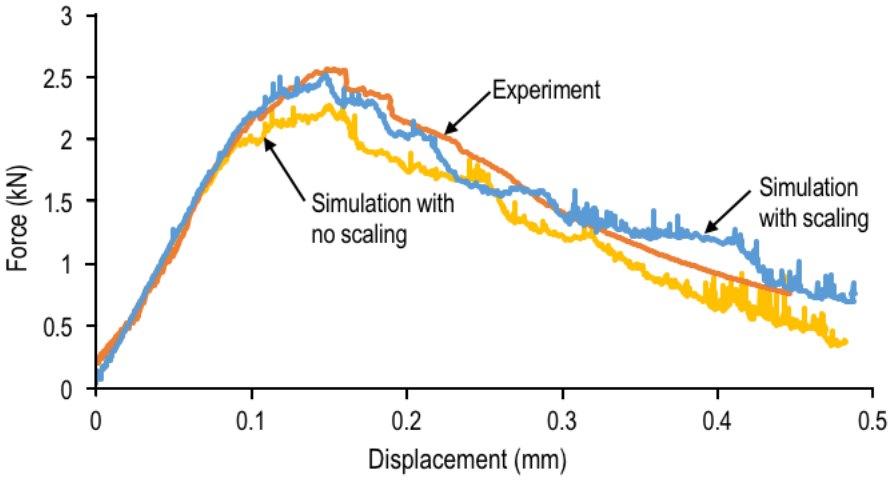

Figure 5.8: Load vs. Displacement plots for experimental results and PFC3D Model for unmodified binder with scaling for size effect considered and direct input from BBR test

Figure 5.8 presents the necessity for scaling the tensile strength determined from the BBR test. SCB experiment and simulation results for unmodified asphalt are shown where simulations were run for two different values of tensile strength shown in Table 4.3. One plot shows the simulation considering size effect and the other inputs the tensile strength directly from the BBR test results. Without scaling the tensile strength, it can be seen that the elastic response is in good agreement with the SCB results but the peak load capacity predicted by the PFC3D model is significantly lower than that obtained form the SCB test. The elastic response predicted by the elastic modulus from experiments on FAM is unchanged and the post-peak responses indicate similar behavior for both simulations.

5.2 Parametric Study

In this section, a parametric study is presented to gain understanding of how the bond behavior would affect the overall mechanical response of the mixtures. The motivations for understanding the relationship between the bond behavior and mixture behavior are twofold: 1) it will allow us to design appropriate laboratory experiments on FAM in order to predict the mixture behavior, and 2) it will help us propose new mix designs to achieve certain desirable behavior of the mixtures. The present parametric study investigates three key model parameters, i.e. the elastic modulus, tensile strength and bond fracture energy. The bond fracture energy is a function of the elastic modulus, tensile strength and parameter α, which is used to determine the decreasing slope of the softening behavior of the constitutive relationship describing the bond.

The fracture energy of the system is a function of the tensile strength, elastic modulus and bond fracture energy of FAM as well as the mean radius of the particles as shown:

$$G_f = \Pi(T, E, G_{f,bond}, R) \tag{5.1}$$

where the mean radius is 4 mm and remains constant as the other parameters change. Dimensionless analysis was performed to explore how the ratio of the fracture energy of the system over sum of the elastic modulus and bond length is related to the ratio of the tensile strength over elastic modulus and the bond fracture energy over the product of the tensile strength and mean bond radius:

$$\frac{G_f}{EL} = \Phi(\frac{T}{E}, \frac{G_{f,bond}}{RT}) \tag{5.2}$$

where L is the bond length used to calculate the bond fracture energy.

The bond fracture energy is a function of the elastic modulus, tensile strength, and value of α and can be re-written to show that the ratio of tensile strength over elastic modulus is related to the ratio of bond fracture energy over the product of the tensile strength and mean bond radius by a constant value for a given specimen:

$$\frac{G_{f,bond}}{RT} = \frac{T^2 L}{2E}(1 + \frac{1}{\alpha})\frac{1}{RT} = \frac{T}{E}\frac{LT}{RT}(1 + \frac{1}{\alpha}) = \frac{T}{E}\frac{L}{R}(1 + \frac{1}{\alpha}) = \gamma\frac{T}{E} \tag{5.3}$$

where $\gamma = \frac{L}{R}(1 + \frac{1}{\alpha})$ and is a constant for a given mixture. L is equal to bond length and assumed to be 1 mm and R is the mean bond radius assumed to be 4 mm. The

value for α is constant for a given mix design.

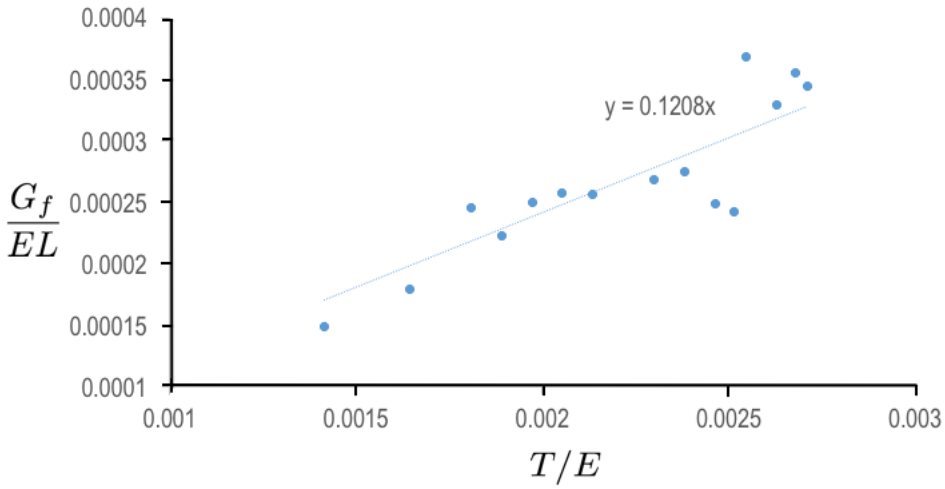

Figure 5.9: Tensile strength over elastic modulus versus fracture energy of the system over sum of the elastic modulus and bond length for varying values of tensile strength for unmodified asphalt mixtures

Since the ratio of the tensile strength over elastic modulus and the bond fracture energy over the product of the tensile strength and mean bond radius are related by a constant, the ratio of the tensile strength over elastic modulus is presented only. Figure 5.9 shows a plot of tensile strength over elastic modulus versus fracture energy of the system over the sum of the elastic modulus and bond length. This parametric study keeps the elastic modulus and α constant which are assumed to be values used for the unmodified elastic modulus of 4.29 GPa and 0.845, respectively. The tensile strength varies for each simulation, which changes the bond fracture energy since it is a function of the tensile strength and constant young's modulus and α. The ratio of fracture energy of the system over the sum of the elastic modulus and bond length changes as the tensile strength is varied. The bond length is kept constant and the system fracture energy increases as the tensile strength is increased. As Figure 5.9 shows, the ratio of the fracture energy of the system over the sum of the elastic modulus and bond length passes through the origin and follows an approximately linear trend as the ratio

of tensile strength over elastic modulus increases.

5.3 Application for Pavement Design

The results from the parametric study can be used as a deign tool for asphalt pavements. The goal for the pavement design is to determine what type and percentage of GNP would be needed to achieve a target strength for a certain low temperature.

Type of GNP			850			4827	
Amount of GNP added	0%	0.5%	1%	3%	0.5%	1%	3%
α	0.845	0.92	0.91	0.93	0.91	0.93	0.92

Table 5.1: Values of α used to determine the required bond fracture energy to fit the simulation to the experimental results

Table 5.1 shows the various values chosen for α to determine the bond fracture energy that fits the post-peak behavior of the simulation to the experimental results. These values range from 0.845 to 0.93 and are higher for asphalt mixtures modified with GNP. For a given type of GNP, the value for α is relatively constant and range from 0.91 to 0.93. For the purpose of the design of asphalt pavements, this value of α can be assumed to be a constant value and can conservatively be chosen to be equal to 1. When α is equal to 1, the bond fracture energy becomes:

$$G_{f,bond} = \frac{T^2 L}{2E} \tag{5.4}$$

The relationship for the tensile strength over elastic modulus versus fracture energy of the system over sum of the elastic modulus and bond length found in the parametric study results in Figure 5.9 can be used to determine what tensile strength is needed to achieve a certain target fracture energy, assuming a constant value for α and a constant elastic modulus. Once a target tensile strength is known, the BBR experiment can be performed on FAM with a certain percentage of GNP to obtain the young's modulus of the mixture. The SCB test can be performed on the mixture with the same amount of GNP to obtain the fitting parameter α. With these values, simulations can be performed to obtain the necessary value of tensile strength to achieve the target fracture energy. Finally, BBR tests can be performed on FAM to determine what percentage of GNP needs to be added to in order to achieve the required tensile strength.

In summary, for a certain elastic modulus and assuming that α is conservatively equal to 1, the relationship between the tensile strength over elastic modulus versus fracture energy of the system over sum of the elastic modulus and bond length can be used to determine what tensile strength is required to achieve a target fracture energy. Then BBR tests can be performed on FAM with various percentages of GNP to determine how much GNP needs to be added to achieve the required tensile strength.

Chapter 6

Conclusion and Discussion

This research explores the application of the simplistic discrete element model for predicting the peak load and post peak behavior for the fracture behavior of asphalt mixtures at low temperatures. The findings of the study can be summarized as follows:

- The use of GNP in asphalt binder exhibits significant increases in strength and fracture energy when compared to unmodified asphalt binder.
- Mixing the GNP and asphalt binder using the high shear mixing technique allows for better dispersion and higher strengths.
- The elastic modulus can be obtained from performing the BBR test on FAM and directly inputted into the discrete element model to yield a reasonable prediction of the elastic response of the mixture.
- The tensile strength of the bond contact of the discrete element model can be obtained from the BBR test result with the size effect adjustment. It is shown that the discrete element model is capable of predicting the peak load capacity of the mixture specimens.
- The analysis of the size effect on the tensile strength of the simulation shows that the peak load capacity is governed by the bond strength.
- The results of the parametric study indicate that the DEM model could be used as a design tool to determine what percentage of GNP is needed to achieve the

necessary tensile strength for a target value of fracture energy

- The post-peak softening response can be captured by employing a softening curve for the bond behavior which requires the input of the bond fracture energy. In order to obtain the energy needed to fracture the bond, more sophisticated experiments on FAM would be required.

References

[1] Hou, Y., Wang, L., Yue, P., Pauli, T., & Sun, W. (2014). Modeling Mode I Cracking Failure in Asphalt Binder by Using Nonconserved Pahse-Field Model. *Journal of Materials in Civil Engineering*, *26*(4), 684–691.

[2] Wang, D., Wang, L., Gu, X., & Zhou, G. (2013). Effect of Basalt Fiber on the Asphalt Binder and Mastic at Low Temperature. *Journal of Materials in Civil Engineering*, *25*(3), 355–364.

[3] Yang, J., & Tighe, S. (2013). A Review of Advances of Nanotechnology in Asphalt Mixtures. *Procedia - Social and Behavioral Sciences*, 1269–1276.

[4] Gu, X., Xu, T., & Ni, F. (2014). Rheological behavior of basalt fiber reinforced asphalt mastic. *J. Wuhan Univ. Technol.-Mat. Sci. Edit. Journal of Wuhan University of Technology-Mater. Sci. Ed.*, *29*(5), 950–955.

[5] Hossain, Z., Zaman, M., Saha, M., & Hawa, T. (2014). Evaluation of Viscosity and Rutting Properties of Nanoclay-Modified Asphalt Binders. *Geo-Congress 2014 Technical Papers*, 3695–3702.

[6] Arabani, M., & Faramarzi, M. (2015). Characterization of CNTs-modified HMA's mechanical properties. *Construction and Building Materials*, *83*, 207–215.

[7] Yan, Y., Cocconcelli, C., Roque, R., Nash, T., Zou, J., Hernando, D., & Lopp, G. (2015). Performance evaluation of alternative polymer-modified asphalt binders. *Road Materials and Pavement Design*, 389-403.

[8] Nanoclays. (n.d.). Retrieved July 31, 2015, *http://www.sigmaaldrich.com/materials-science/nanomaterials/nanoclay-building.html*

[9] Yao, H., Li, L., Xie, H., Dan, H., & Yang, X. (2011). Microstructure and Performance Analysis of Nanomaterials Modified Asphalt. *Road Materials and New Innovations in Pavement Engineering.*

[10] Jahromi S., & Ghaffarpour, K.A. (2009). Effects of Nanoclay on Rheological Properties of Bitumen Binder. *Construction and Building Materials*, *23*, 2894-2904.

[11] Zare-Shahabadi, A., Shokuhfar, A., & Ebrahimi-Nejad, S. (2010). Preparation and Rheological Characterization of Asphalt Binders Reinforced with Layered Silicate Nanoparticles. *Construction and Building Materials, 24*(7), 1239-1244.

[12] Nazzal, M., Kaya, S., Gunay, T., & Ahmedzade, P. (2013). Fundamental Characterization of Asphalt Clay Nanocomposites. *Journal of Nanomechanics and Micromechanics J. Nanomech. Micromech.*, *3*(1), 1-8.

[13] Abdelrahman, M., Katti, D., Ghavibazoo, A., Upadhyay, H., & Katti, K. (2014). Engineering Physical Properties of Asphalt Binders through Nanoclay?Asphalt Interactions. *J. Mater. Civ. Eng. Journal of Materials in Civil Engineering*, *26*(12), 04014099

[14] Mun, S., & Lee, H. (2011). Modeling Viscoelastic Crack Growth in Hot-Mix Asphalt Concrete Mixtures Using a Disk-Shaped Compact Tension Test. *J. Eng. Mech.*, *137*(6), 431-438.

[15] Barik, T. K., Sahu, B, & Swain, V. (2008) Nanosilica-from medicine to pest control Parasitol. *Parisitol Res, 103*, 253-8.

[16] Yao, H., You, Z., Li, L., Lee, C., Wingard, D., Yap, et. al. (2013). Rheological Properties and Chemical Bonding of Asphalt Modified with Nanosilica. *J. Mater. Civ. Eng. Journal of Materials in Civil Engineering*, *25*(11), 1619-1630.

[17] Yusoff, N., Breem, A., Alattug, H., Hamim, A., & Ahmad, J. (2014). The effects of moisture susceptibility and aging conditions on nano-silica/polymer-modified asphalt mixtures. *Construction and Building Materials*, *72*, 139-147.

[18] Al-Adham, K., & Arifuzzaman, M. (2014). Moisture damage evaluation in carbon nanotubes reinforced asphalts. Sustainability, Eco-efficiency, and Conservation in Transportation Infrastructure Asset Management, 103-109.

[19] Shirakawa, T., Tada, A. & Okazaki, N. (2012). Development of functional carbon nanotubes-asphalt composites. *International Journal of GEOMATE*, *2*(1), 161-165.

[20] Basalt Fiber Properties, Advantages and Disadvantages. (n.d.). Retrieved July 31, 2015. http://www.build-on-prince.com/basalt-fiber.html#sthash.1bkllF7E.dpbs

[21] Zheng, Y., Cai, Y., Zhang, G., & Fang, H. (2014). Fatigue property of basalt fiber-modified asphalt mixture under complicated environment. J. Wuhan Univ. Technol.-Mat. Sci. Edit. *Journal of Wuhan University of Technology-Mater. Sci. Ed.*, *29*(5), 996-1004.

[22] Gao, C., Han, S., Chen, S., & Li, H. (2014). Research on Basalt Fiber Asphalt Concrete's Low Temperature Performance. *AMM Applied Mechanics and Materials*, 505-506, 35-38.

[23] Novoselov, K.S., Geim, A. K., Morozov, S.V., Jiang, D., Katsnelson, M. I., Grigorieva, I. V., Dubonos, S. V., & Firsov, A. A. (2005) Two-dimensional gas of massless Dirac fermions in graphene. *Nature*, *438*, 197.

[24] Zhang, Y., Tan, Y. W., Stormer, H. L., & Kim, P. (2005) Experimental observation of the quantum Hall effect and Berry's phase in graphene. *Nature*, emph438, 201.

[25] Lee, C., Wei, X., Kysar, J. W., & Hone, J. (2008) Measurement of the elastic properties and intrinsic strength of monolayer graphene. *Science*, *321*, 385.

[26] Kim, K., Regan, W., Geng, B., Aleman, B., Kessler, B. M., Wang, F., Crommie, M. F., & Zettl, A. (2010) High-temperature stability of suspended single-layer graphene. *Phys. Status Solidi, RRL4*, *11*, 302-304.

[27] Kim, Y., Allen, D., & Little, D. (2005). Damage-Induced Modeling of Asphalt Mixtures through Computational Micromechanics and Cohesive Zone Fracture. *J. Mater. Civ. Eng. Journal of Materials in Civil Engineering*, *17*(5), 477–484.

[28] Arago, F., & Kim, Y. (2010) Modeling Fracture and Failure of Heterogeneous and Inelastic Asphaltic Materials Using the Cohesive Zone Concept and the Finite Element Method. *GeoFlorida 2010*, 2662–2671.

[29] Huang, H., Lecampion, B., & Detournay, E. (2012). Discrete element modeling of tool-rock interaction I: Rock cutting. *Int. J. Numer. Anal. Meth. Geomech. International Journal for Numerical and Analytical Methods in Geomechanics*, *37*, 1913-1929.

[30] Ban, H., Kim, Y., & Rhee, S. (2012). Computational microstructure modeling to estimate progressive moisture damage behavior of asphaltic paving mixtures. *Int. J. Numer. Anal. Meth. Geomech. International Journal for Numerical and Analytical Methods in Geomechanics*, *37*(13), 2005-2020.

[31] Dugdale, DS. (1960). Yielding of steel sheets continuity slits. *J. Mech. Phys. Solids, 8*(2),100-104.

[32] Barrenblatt, GI. (1959). The mathematical theory of equilibrium of cracks in brittle fracture. *Adv. Appl. Mech.*, *7*, 55?129.

[33] Bazant, Z. P. & Planas, J. (1989). Fracture and size effect in concrete and other quasibrittle materials. *CRC Press*, Boca Raton and London.

[34] Im, S., Ban, H., & Kim, Y. (2014). Rutting and cracking modeling of asphalt pavements considering nonlinear viscoelasticity and cohesive zone fracture. *Asphalt Pavements,* 775-783.

[35] Schillinger, D., Borden, M.J., & Stolarski, H.K. (2015). Isogeometric collocation for phase-field fracture models. *Computer Methods in Applied Mechanics and Engineering*, *284*, 583-610.

[36] Borden, M.J., Verhoosel, C.V., Scott, M.A., Hughes, T.J.R., & Landis,C.M. (2012). A phase-field description of dynamic brittle fracture. *Computer Methods in Applied Mechanics and Engineering, 217-220*,77-95.

[37] Cusatis, G., Baant, Z. P. & Cedolin, L. (2003). Confinement-shear lattice model for concrete damage in tension and compression: I. Theory. *Journal of Engineering Mechanics ASCE*, *129*(12), 1439–1448.

[38] Cusatis, G., Baant, Z. P. & Cedolin, L. (2003). Confinement-Shear Lattice Model for Concrete Damage in Tension and Compression: II. *Computation and Validation. J. Eng. Mech. Journal of Engineering Mechanics*, *129*(12), 1449-1458.

[39] Cundall, P.A. & Strack, O. D. L. (1979). A discrete numerical model for granular assemblies. *Geotechnique*, *29*, 47–65

[40] Liliu, G., & van Mier, J. G. M. (2003). 3d lattice type fracture model for concrete. *Engineering Fracture Mechanics*, *70*, 927–941.

[41] Schauffert, E. A. & Cusatis, G. (2011). Lattice discrete particle model for fiber-reinforced concrete. I: Theory. *Journal of Engineering Mechanics ASCE*, *138*(7), 826–833.

[42] Zubelewicz, A. & Bazant, Z. P. (1987). Interface modeling of fracture in aggregate composites. *Journal of Engineering Mechanics ASCE*, *113*(11), 1619–1630.

[43] Abbas, A., Papagiannakis, A., & Masad, E. (2005). Micromechanical Simulation of Asphaltic Materials Using the Discrete Element Method. *Asphalt Concrete*, 1–11.

[44] Hyunwook, K., & Buttlar, W. G. (2009). Discrete Fracture Modeling of Asphalt Concrete. *International Journal of Solids and Structures*, emph46(13), 2593–604.

[45] Aragao, F., Kim, Y., Lee, J., & Allen, D. (2011) Micromechanical Model for Heterogeneous Asphalt Concrete Mixtures Subjected to Fracture Failure. *J. Mater. Civ. Eng. Journal of Materials in Civil Engineering*, *23*(1), 30–38.

[46] Potyondy, D. (June 23, 2016). Material-Modeling Support in PFC [via fistPkg23]. *Itasca Consulting Group, Inc. Minneapolis, MN, Technical Memorandum ICG7766-L.*

[47] Potyondy, D. O., & Cundall. P. A. (2004). A Bonded-particle Model for Rock. *International Journal of Rock Mechanics and Mining Sciences*, *41*(8), 1329–1364.

[48] Bazant, Z. P., Vorechovsky, M., & Novak, D. (2007). Energetic-statistical size effect simulated by SFEM with stratified sampling and crack band model. *International Journal for Numerical Methods in Engineering*, *71*, 1297–1320.

[49] Marasteanu M., Cannone Falchetto, A., Turos, M., & Le, J.-L. (2012). Development of a simple test to determine the low temperature strength of asphalt mixtures and binders. *NCHRP-IDEA Program Project Final Report.*

[50] Sousa, P., Kassem, E., Masad, E., and Little, D. (2013). New design method of fine aggregate mixtures and automated method for analysis of dynamic mechanical characterization data. *Journal of Construction and Building Materials*, *41*, 216–223.

[51] American Association of State Highway and Transportation Officials. AASHTO T240-09-UL. (2009). Test for effect of heat and air on a moving film of asphalt (Rolling Thin-Film Oven Test).

[52] American Association of State Highway and Transportation Officials. AASHTO R028-09-UL. (2009). Standard Practice for Accelerated Aging of Asphalt Binder Using a Pressurized Aging Vessel (PAV).

[53] American Association of State Highway and Transportation Officials. AASHTO T313-10-UL. (2010). Determining the Flexural Creep Stiffness of Asphalt Binder Using the Bending Beam Rheometer (BBR).

[54] American Association of State Highway and Transportation Officials. (2013). AASHTO TP 105 Standard Method of Test for Determining the Fracture Energy of Asphalt Mixtures Using the Semicircular Bend Geometry (SCB).

[55] Li, X., & Marasteanu, M.O. (2010) The fracture process zone in asphalt mixture at low temperature. *Engineering Fracture Mechanics*, *77*, 1175–1190.

[56] Zegeye, E., Le, J.-L., Turos, M. & Marasteanu, M.O. (2012). Investigation of size effect in asphalt mixture fracture testing at low temperature. *Road Materials and Pavement Design*, *13*, 88–101.

[57] Le, J.-L., Cannone Falchetto, A., & Marasteanu, M. O. (2013) Determination of strength distribution of quasibrittle structures from size effect analysis. *Mechanics of Materials*, *66*, 79–87.

[58] Cannone Falchetto, A., Le, J.-L., Turos, M. I., & Marasteanu, M. O. (2014). Indirect determination of size effect on strength of asphalt mixture at low temperatures. *Materials and Structures*, *47*(1-2), 157–169.

[59] Bazant, Z. P. (2005). Scaling of structural strength. Elsevier, London.

[60] Marasteanu, M.O., Zofka, A., Turos, M., Li, X., Velasquez, R,. Li, X., Buttlar, W., Paulino, G., Braham, A., Dave, E., Ojo, J., Bahia, H., Bausano, C. J., Gallistel, A., & McGraw, J. (2007) Investigation of Low Temperature Cracking in Asphalt Pavements: National Pooled Fund Study 776. *Final Report. Minnesota Department of Transportation, St. Paul*.

[61] Azevedo, N., Lemos, J., & Almeida, J. (2010). A Discrete Element Model For The Fracture Analysis of Reinforced Concrete. *III European Conference on Computational Mechanics.*

[62] Cusatis, G., Pelessone, D., & Mencarelli, A. (2011). Lattice Discrete Particle Model (LDPM) for failure behavior of concrete. I: Theory. *Cement and Concrete Composites*, *33*(9), 881-890.

[63] Hillerborg, A., Modeer, M. & Petersson, PE. (1976). Analysis of crack formation and crack growth in concrete by means of fracture mechanics and finite elements. *Cem. Concr. Res.*, *6*(6), 773?781.

Appendix A

Appendix

Sieve Size (mm)	Composite Formula
25.0	
19.0	
12.5	
9.5	100
4.75	69
2.36	52
1.18	43
0.6	27
0.3	14
0.15	8
0.075	4.7
Spec. Voids	4.0
%AC	5.5

Table A.1: Asphalt Mix Design